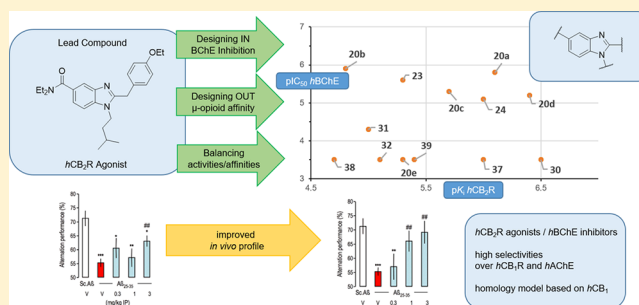


## Structure–Activity Relationships and Computational Investigations into the Development of Potent and Balanced Dual-Acting Butyrylcholinesterase Inhibitors and Human Cannabinoid Receptor 2 Ligands with Pro-Cognitive in Vivo Profiles

Dominik Dolles,<sup>†</sup> Matthias Hoffmann,<sup>†</sup> Sandra Gunesch,<sup>†</sup> Oliviero Marinelli,<sup>‡</sup> Jan Möller,<sup>§</sup> Giorgio Santoni,<sup>‡</sup> Arnaud Chatonnet,<sup>||</sup> Martin J. Lohse,<sup>§</sup> Hans-Joachim Wittmann,<sup>⊥</sup> Andrea Strasser,<sup>⊥</sup> Massimo Nabissi,<sup>‡</sup> Tangui Maurice,<sup>#</sup> and Michael Decker<sup>\*,†,||</sup><sup>†</sup>Pharmaceutical and Medicinal Chemistry, Institute of Pharmacy and Food Chemistry, Julius Maximilian University of Würzburg, Am Hubland, D-97074 Würzburg, Germany<sup>‡</sup>School of Pharmacy, Department of Experimental Medicine, University of Camerino, I-62032 Camerino, Italy<sup>§</sup>Institute of Pharmacology and Toxicology, Julius Maximilian University of Würzburg, Versbacher Strabe 9, D-97078 Würzburg, Germany<sup>||</sup>INRA UMR866, University of Montpellier, F-34060 Montpellier, France<sup>⊥</sup>Pharmaceutical and Medicinal Chemistry II, Institute of Pharmacy, University of Regensburg, D-95053 Regensburg, Germany<sup>#</sup>INSERM UMR-S1198, University of Montpellier, EPHE, F-34095 Montpellier, France

## Supporting Information

**ABSTRACT:** The enzyme butyrylcholinesterase (BChE) and the human cannabinoid receptor 2 ( $hCB_2R$ ) represent promising targets for pharmacotherapy in the later stages of Alzheimer's disease. We merged pharmacophores for both targets into small benzimidazole-based molecules, investigated SARs, and identified several dual-acting ligands with a balanced affinity/inhibitory activity and an excellent selectivity over both  $hCB_1R$  and  $hAChE$ . A homology model for the  $hCB_2R$  was developed based on the  $hCB_1R$  crystal structure and used for molecular dynamics studies to investigate binding modes. In vitro studies proved  $hCB_2R$  agonism. Unwanted  $\mu$ -opioid receptor affinity could be designed out. One well-balanced dual-acting and selective  $hBChE$  inhibitor/ $hCB_2R$  agonist showed superior in vivo activity over the lead  $CB_2$  agonist with regards to cognition improvement. The data shows the possibility to combine a small molecule with selective and balanced GPCR-activity/enzyme inhibition and in vivo activity for the therapy of AD and may help to rationalize the development of other dual-acting ligands.



## INTRODUCTION

Alzheimer's disease (AD) is the most common form of dementia. According to the annual World Alzheimer Report, there are more than 47 million people suffering from AD. By 2050, researchers expect this number to climb up to even more than 130 million.<sup>1</sup> Currently, a cure is pending and pharmacotherapy is very limited. Three acetylcholinesterase (AChE) inhibitors (rivastigmine, donepezil, and galantamine) and one *N*-methyl-D-aspartate receptor (NMDA) antagonist (memantine) are currently available as drugs. Unfortunately, these drugs are only effective in early stages of AD, and they only act symptomatically but do not slow down progression or even cure AD.<sup>2</sup>

The reasons for an outbreak of this complex disease still remain unknown. AD is pathobiologically characterized by the presence of senile plaques, which consist of  $\beta$ -amyloid ( $A\beta$ ).  $A\beta$  is an insoluble peptide and is formed by  $\beta/\gamma$ -secretase-induced cleavage of the amyloid precursor protein (APP). Another hallmark is the

formation of neurofibrillary tangles, which consist of hyperphosphorylated  $\tau$ -protein aggregates. Once formed, both  $A\beta$  and  $\tau$ -proteins trigger the progressive loss of muscarinic neurons in the brain and lead to memory deficits and cognitive dysfunction.<sup>3–5</sup> Moreover,  $A\beta$  induces activation of neuroinflammatory pathways characterized by activated microglia and astrocytes as observed in the brains of AD patients.<sup>6</sup> Neuroinflammation then leads to the production of pro-inflammatory chemokines, cytokines, and neurotoxins, which speed up AD progression by themselves.<sup>7</sup> The exact sequence of these cascade processes is still under discussion.

In the past years, the human cannabinoid receptors ( $hCBRs$ ) were identified as targets for drug development concerning neurodegenerative disorders. Currently, there are two known subtypes:

Received: November 29, 2017

the human cannabinoid receptors 1 ( $hCB_1R$ ) and 2 ( $hCB_2R$ ).  $hCB_1Rs$  are mainly expressed in the brain;  $hCB_2Rs$  were first described in the peripheral immune system<sup>9</sup> and then described to occur to a lower extent in the central nervous system (CNS), especially microglia.<sup>10,11</sup> In the course of AD, expression levels of  $hCB_1R$  do not change, but overexpression of  $hCB_2R$  is observed in certain brain regions (especially in the hippocampus) of AD patients.<sup>12</sup> Furthermore,  $CB_2R$  expression is associated with microglia and astrocytes that are surrounded by neuritic plaques.<sup>13</sup> The theory that up-regulation of  $CB_2R$  signaling leads to reduction of associated inflammatory processes<sup>14</sup> was substantiated in several in vitro studies:  $hCB_2R$  agonists reduce the production of neurotoxic factors, such as reactive oxygen species (ROS) and pro-inflammatory mediators (TNF- $\alpha$  and cytokines).<sup>15–17</sup> Furthermore, in vivo studies support the therapeutic potential of  $hCB_2R$  agonists: Wu et al. injected  $A\beta_{1–40}$  intracerebrally into rat brains and then treated the animals with MDA7, a known  $hCB_2R$  agonist. After 14 days, behavioral tests were performed (place learning in the Morris water maze) and the rat brains slices were then examined. MDA7 was found to promote  $A\beta$  clearance, to decrease secretion of proinflammatory mediators and ultimately led to restored synaptic plasticity, cognition, and memory.<sup>18</sup> In another study, transgenic Tg2576 mice that overexpress APP were continuously treated with JWH-133, another known  $hCB_2R$  agonist, at different stages of AD. As a result,  $A\beta$  production was lowered, reactive microglia cells were reduced, and a positive cognitive performance was observed.<sup>19</sup> The importance of  $CB_2R$  in  $A\beta$  formation was shown in J20APP mice (overexpression of APP in neocortex and hippocampus). Deletion of  $CB_2R$  led to an increased formation and deposition of  $A\beta$ , which supports  $CB_2R$ 's role as a reducing agent of  $A\beta$ .<sup>20</sup> In summary, activation of  $hCB_2R$  leads to various beneficial effects concerning AD and additionally seems to play a central role in other neurodegenerative diseases such as Parkinson's and Huntington's disease.<sup>21</sup>

The oldest theory regarding AD pathophysiology is the “cholinergic hypothesis”, which describes the massive loss of cholinergic neurons in AD.<sup>22</sup> The amount of acetylcholinesterase (AChE), the metabolizing enzyme of the neurotransmitter acetylcholine (ACh), decreases in the course of AD. However, the concentration of its isoenzyme butyrylcholinesterase (BChE) stays unchanged or even increases and is able to compensate for the loss of AChE, since BChE can also hydrolyze ACh into choline and acetate.<sup>23,24</sup> Besides that, it was shown that BChE (over-) expression is associated with senile plaques and the transformation of nonfibrillar to fibrillary  $A\beta$  plaques.<sup>25,26</sup> Inhibition of BChE is therefore a promising approach when it comes to combat AD's cognitive deficits, especially in later stages when AChE diminishes.<sup>27</sup> In a very recent in vivo study, BChE knockout mice showed enhanced learning abilities in memory tests as compared to wildtype littermates, and after intercerebroventricular injections of  $A\beta_{25–35}$  oligomers, BChE knockout mice appeared less sensitive to the learning and memory deficits, oxidative stress, and decrease in hippocampal ACh, as induced by the amyloid peptide in wildtype animals.<sup>28</sup> In another study, a sulfonamide-based nanomolar BChE inhibitor was investigated. In one of the very few in vivo studies that applied BChE-selective inhibitors, mice treated with this inhibitor showed improved memory and learning abilities in passive avoidance and Morris water maze tests without producing acute cholinergic adverse effects.<sup>29</sup>

Furthermore, it is remarkable that there's a colocalization of BChE and  $hCB_2Rs$  in microglia cells of the pathophysiologically altered brain. Glia cells play an important role in production of BChE and can be specifically targeted by  $CB_2R$  agonists.<sup>30,31</sup>

The multifactorial character of AD makes it difficult if not impossible to apply the classical “one target—one disease” for successful drug development.<sup>32</sup> It is therefore advantageous to develop multitarget drugs, which address different targets simultaneously. These drugs consist of two drug entities either as a hybrid linked by a spacer<sup>33</sup> or merged into one single entity;<sup>32,34–36</sup> for the latter case, only a few successful examples have been described. (For a review, see ref 35.) Hybrids addressing CBRs as one of the targets have been developed successfully.<sup>37–39</sup> In a remarkable recent work, Rampa et al. have achieved inhibiting both  $hBChE$  and fatty acid amide hydrolase (FAAH) and therefore target both the endocannabinoid and cholinergic system.<sup>40</sup> The main disadvantage of hybrid molecules is their (often) high molecular weight, which goes along with a violation of Lipinski's rule of five.<sup>41</sup> In contrast, merged ligands are still “small molecules” and their molar mass remains often at the same level as the “single compound”.<sup>35,36</sup> In return, their development is more laborious. Both drug moieties have to be “fused” into one entity. The problem is that, if affinity is increased at one target, it is very likely decreased at the other one.<sup>36,37</sup> There are three common approaches to obtain such merged/dual-acting compounds: “designing in”, “designing out”, and “balancing”. The most common approach is “designing in”, where structural elements of two highly selective ligands are combined in one molecule, and the resulting compound then incorporates activity at the two desired targets. In a second approach, a merged compound not only possesses activity for two desired targets but also shows undesirable activity at a third target. In this case, “designing out” aims for excluding activity at the third, undesired target but keeping activity at the other two desired ones. In the third approach, a compound shows a very high affinity for one target but only moderate activity for the other target. Here, the aim is to balance the affinity at both desired targets.<sup>32,35</sup> Despite these difficulties, there are already several successful examples for merged ligands in the recent literature, such as adenosine  $A_{2A}$  receptor/monoamine oxidase B ligands and human histamine  $H_3$  receptor antagonists/AChE inhibitors developed in our group; the latter proved successful even in vivo.<sup>42,43</sup>

In our previous work,<sup>36</sup> we applied a novel pharmacophore model for BChE inhibitors to several benzimidazole-based selective  $hCB_2R$  agonists initially developed by AstraZeneca A (Figure 1)<sup>44</sup> in a “designing in” approach. A related merged structure based on indazole had been described before.<sup>45</sup> After the synthesis of various heterocyclic templates and applying various substitution patterns, we had obtained a first substance library and some compounds showed activity in the (sub)micromolar range at both targets and an excellent selectivity over both  $hCB_1R$  and AChE (Figure 1).<sup>36</sup> Furthermore, we conducted molecular dynamics (MD) simulations in both  $hCB_2R$  and BChE, which gave the first insights into the binding mode of our lead compounds A and B and helped the understanding of structure–activity relationships (SARs) at both targets.

In the present study, we developed our compound portfolio further by balancing activities at  $hCB_2R$  and BChE and by investigating and designing out unwanted interactions with the  $\mu$  opioid receptor (MOP). We synthesized and characterized in a portfolio of in vitro assays 13 novel dual-acting  $hCB_2R$  ligands and BChE inhibitors. We furthermore investigated for the first time intrinsic activities at the  $hCB_2R$  for second and third generation compounds. Finally, we evaluated the ability of our second generation lead compound B to fight cognition deficits induced by intracerebroventricular (ICV)  $A\beta_{25–35}$  injections in mice, as an in vivo pharmacological model for AD.

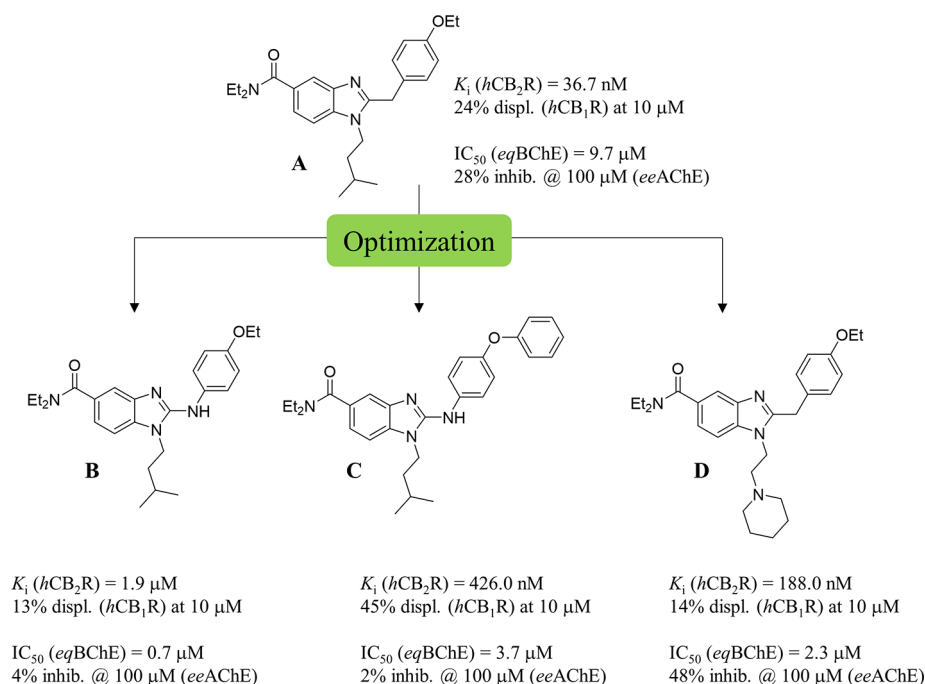


**Figure 1.** Development of the second generation lead structures B, C, and D starting from AstraZeneca's selective  $hCB_2R$  agonist A, the first generation lead.<sup>36,44</sup>

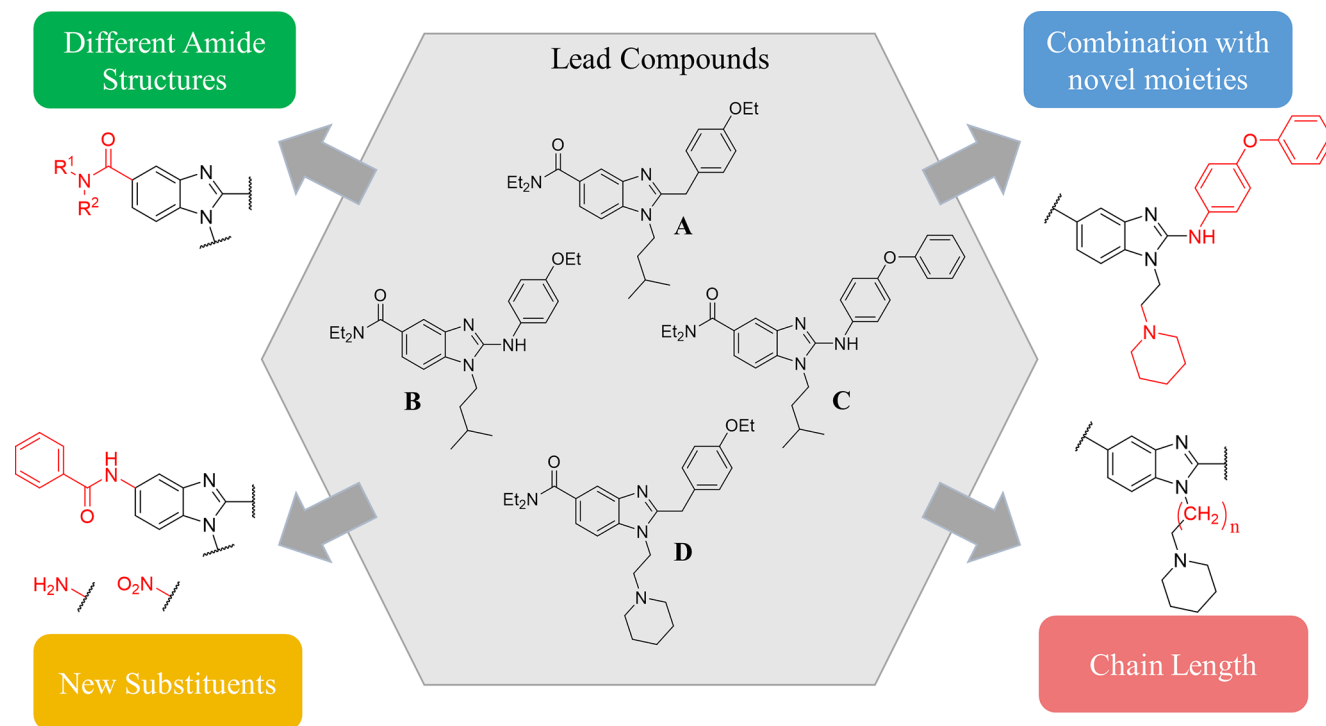


**Figure 2.** Structural compound design approaches carried out starting from lead compounds A–D.

## RESULTS

**Chemistry.** The difficulty in designing a multitarget compound is to “fuse” drug entities and at the same time to keep or even improve the activity at both targets. The starting point for advanced synthetic approaches are Astra Zeneca's benzimidazole A as well as our second generation lead compounds B, C, and D described very recently (Figures 1 and 2).<sup>36,44</sup> These compounds already showed either a high affinity at one of the two targets or even a balanced micromolar activity profile. From these results, we followed several design approaches (Figure 2): the introduction of

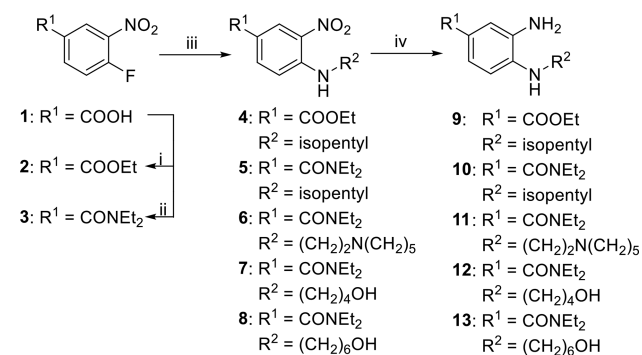
different amides (green) and substituents (yellow) at position 5 of the benzimidazole core, alternation of the chain length (red), and a combination of the most promising substitution patterns (blue). Before, we also had synthesized other heterocyclic templates such as amino-indazoles, but the compounds lost affinity at all targets.<sup>36</sup> Therefore, we returned to the initial structural template.

The necessity of a (diethyl)amide for a high  $hCB_2R$  affinity had been previously demonstrated,<sup>36,44</sup> but data for inhibition of either AChE or BChE of several amides was not available. The

electron-withdrawing character of amides led us using substituents with different electronic effects (e.g., nitro and amino) at position 5 of the benzimidazole core. Ethylenepiperidinyl substitution at the  $N^1$  of the benzimidazole core already caused (sub)micromolar activity at both  $hCB_2R$  and BChE. The aim was to extend the alkylene chain and to increase lipophilicity and interaction between the side chain and the oxyanion hole of the BChE.<sup>36</sup> Lastly, we combined the most promising substituents in order to increase dual-activity.

Specifically, the synthesis of benzimidazoles and 2-amino benzimidazoles was carried out as previously reported starting from 4-fluoro-3-nitrobenzoic acid **1**.<sup>36</sup> To introduce the different amide moieties in the last step, esterification was performed to obtain ester **2**. For the synthesis of target compounds **23**, **24**, and **30–32**, the diethylamide moiety **3** was formed using HBTU as the coupling agent. In the next step, nucleophilic substitution with various amines afforded compounds **4–8**. Reduction of the nitro group was achieved using tin(II) to obtain *o*-phenylenediamines **9–13** (Scheme 1).

**Scheme 1. Synthesis of *o*-Phenylene Diamine Precursors 9–13<sup>a</sup>**



<sup>a</sup>Conditions: (i)  $\text{H}_2\text{SO}_4$ , EtOH, reflux, 24 h; (ii)  $\text{HNEt}_2$ ,  $(\text{COCl})_2$ ,  $\text{NEt}_3$ , DMF, 0 °C to rt, 5 h; (iii)  $\text{NHR}^2$ ,  $\text{NEt}_3$ , EtOH, rt, 3 h; (iv)  $\text{SnCl}_2 \cdot 2\text{H}_2\text{O}$ , EtOH, reflux, 6 h.

To obtain benzimidazoles with various amide moieties and spacer lengths, diamines **9**, **12**, and **13** were coupled with

2-(4-ethoxyphenyl)acetic acid to afford compounds **14–16**. Cyclization was achieved in glacial acetic acid, and benzimidazoles **17–19** were obtained in quantitative yields. Ester **17** was hydrolyzed under basic conditions and then coupled with various amines using HBTU as a coupling agent. After purification, amides **20a–e** were obtained in high yields. For various spacer lengths, hydroxy compounds **18** and **19** were treated in an Appel-like reaction with phosphorus tribromide to obtain the bromo compounds **21** and **22**. In the last step, bromine was substituted with piperidine under basic conditions to afford compounds **23** and **24** (Scheme 2).

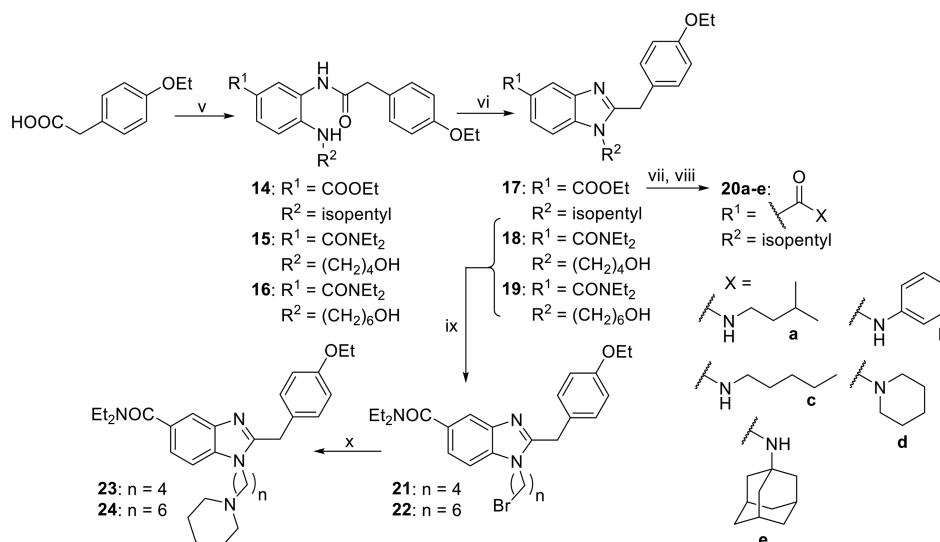
The synthesis of 2-amino benzimidazoles was performed as previously reported.<sup>36</sup> Upon reaction of benzylic and anilinic amines **25a–c** with carbon disulfide, isothiocyanates **26a–c** were obtained.<sup>46</sup> Thiourea derivatives **27–29** were afforded by reacting the respective isothiocyanates with *o*-phenylenediamine **10** or **11**. Cyclization was carried out using EDCI as a coupling reagent, and 2-amino benzimidazoles **30–32** were obtained (Scheme 3).

For the introduction of electron-withdrawing/donating functions at position 5 of the benzimidazole core, a different synthetic approach was applied. Starting from 1-chloro-2,4-dinitrobenzene **33**, nucleophilic substitution with isopentylamine led to compound **34** in quantitative yields. Selective reduction of the 2-nitro moiety to obtain *o*-phenylenediamine **35** was carried out according to Freitag et al.<sup>47</sup> using sodium sulfide as a reducing agent. Amide coupling and cyclization were carried out as described above. 5-Nitro benzimidazole **37** was reduced by tin(II) to afford 5-amino benzimidazole **38**. In the final step, HBTU-mediated amide coupling with benzoic acid afforded compound **39** (Scheme 4).

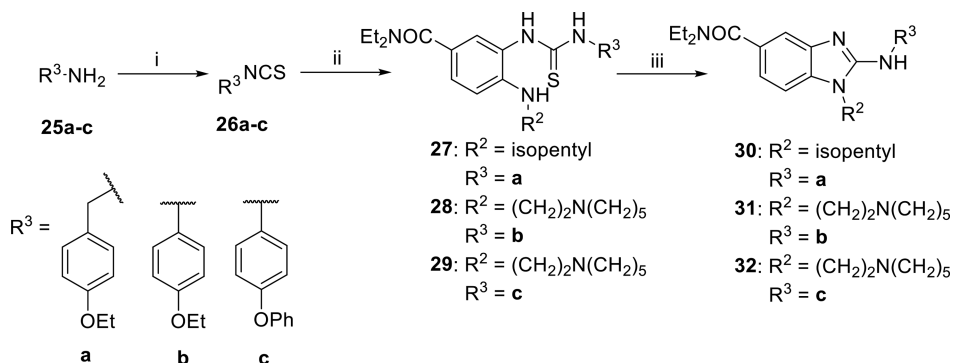
#### Pharmacological Profile of Dual-Acting Compounds.

All target compounds were tested for affinity to  $hCB_1R$  and  $hCB_2R$  in radioligand binding studies (HEK cells stably expressing  $hCB_2R$ ; CHO cells stably expressing  $hCB_1R$ ). Inhibition of AChE (*ee*AChE, E.C.3.1.1.7, from electric eels and *hAChE*, E.C.3.1.1.7, from humans) and BChE (*hBChE*, E.C.3.1.1.8, from humans) was evaluated in the colorimetric Ellman's assay (Table 1). Sequence alignment had shown that the isoform *ee*AChE exhibits a very high sequence homology to the human enzyme (88% sequence identity)<sup>48</sup> (Table 1).

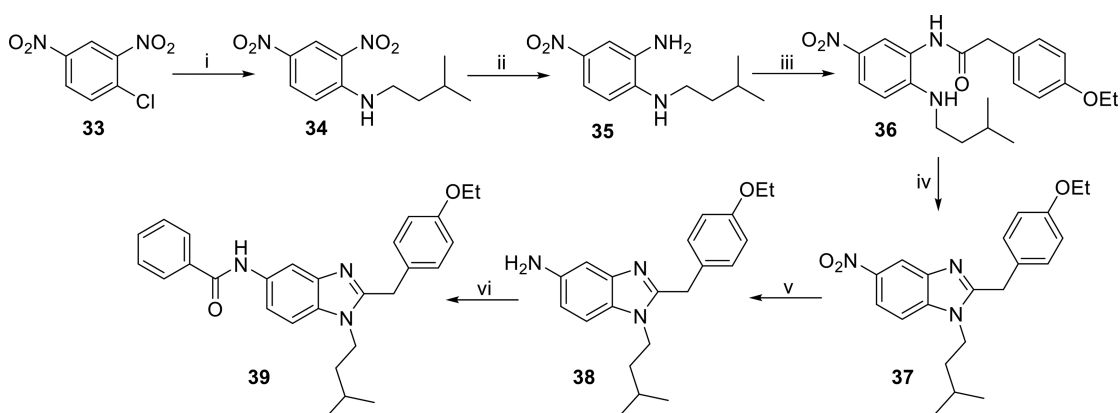
**Scheme 2. Synthesis of Benzimidazoles with Different Amide Moieties or Spacer Lengths<sup>a</sup>**



<sup>a</sup>Conditions: (v) *o*-phenylene diamine **9**, **12**, or **13**, HBTU,  $\text{NEt}_3$ , DMF, rt, 24 h; (vi) AcOH, reflux, 2 h; (vii) LiOH, THF/ $\text{H}_2\text{O}$ , rt, 24 h; (viii) primary and secondary amines **a–e**, HBTU,  $\text{NEt}_3$ , DMF, rt, 24 h; (ix)  $\text{PBr}_3$ ,  $\text{CH}_2\text{Cl}_2$ , 0 °C to rt, 12 h; (x) piperidine,  $\text{K}_2\text{CO}_3$ , DMF, 70 °C, 12 h.

Scheme 3. Synthesis of 2-Amino Benzimidazoles<sup>a</sup>

<sup>a</sup>Conditions: (i) CS<sub>2</sub>, NEt<sub>3</sub>, Boc<sub>2</sub>O, THF, 0 °C to rt, 12 h; (ii) *o*-phenylene diamine **10** or **11**, THF, rt, 6 h; (iii) EDCl·HCl, NEt<sub>3</sub>, THF, reflux, 5 h.

Scheme 4. Synthesis of Benzimidazoles with Electron-Withdrawing/Donating Substituents at Position 5<sup>a</sup>

<sup>a</sup>Conditions: (i) isopentylamine, NEt<sub>3</sub>, EtOH, rt, 24 h; (ii) Na<sub>2</sub>S·H<sub>2</sub>O, NaHCO<sub>3</sub>, MeOH/H<sub>2</sub>O, reflux, 4 h; (iii) 2-(4-ethoxyphenyl)acetic, HBTU, NEt<sub>3</sub>, DMF, rt, 12 h; (iv) AcOH, reflux, 6 h; (v) SnCl<sub>4</sub>·2H<sub>2</sub>O, EtOH, reflux, 6 h; (vi) benzoic acid, HBTU, NEt<sub>3</sub>, DMF, rt, 6 h.

In the first set of compounds, we kept the benzimidazole scaffold of lead compound **A** and introduced different amide moieties at position 5 of the benzimidazole core (**20a–d**). While **20c**, with a straight *N*-alkyl chain, shows a low micromolar affinity toward *h*CB<sub>2</sub>R and a micromolar inhibition of BChE, compound **20a**, with a branched *N*-alkyl chain, shows a micromolar inhibition of BChE as well as a submicromolar affinity toward *h*CB<sub>2</sub>R (**20a**,  $K_i(hCB_2R) = 763.3$  nM and  $IC_{50}(hBChE) = 1.6$   $\mu$ M; **20c**,  $K_i(hCB_2R) = 1.9$   $\mu$ M and  $IC_{50}(hBChE) = 5.2$   $\mu$ M; **Table 1**). When we replaced the straight/branched *N*-alkyl chains with a 1-piperidinyl amide (**20d**), the activity at BChE did not change, but the affinity for *h*CB<sub>2</sub>R could be increased (**20d**,  $K_i(hCB_2R) = 384.5$  nM and  $IC_{50}(hBChE) = 5.7$   $\mu$ M; **Table 1**). It is furthermore remarkable that the introduction of a 1-piperidinyl amide (**20d**), which is similar to AstraZeneca's benzimidazole **A**, resulted in some, albeit moderate, regain in affinity toward *h*CB<sub>1</sub>R ( $K_i(hCB_1R) = 17.0$   $\mu$ M; **Table 1**). The introduction of a sterically demanding 1-adamantyl amide scaffold (**20e**), a typical CB pharmacophore, resulted in a complete loss of activity at both ChEs. The affinity at *h*CB<sub>2</sub>R still was in the micromolar range (**20e**,  $K_i(hCB_2R) = 4.7$   $\mu$ M; **Table 1**), which suggests a tolerance of *h*CB<sub>2</sub>R concerning bulky and nonpolar substituents at position 5 of the benzimidazole core. Lastly, we introduced an aniline amide (**20b**), which kept micromolar activity at BChE but led to an approximately 10-fold decreased affinity at *h*CB<sub>2</sub>R compared to other investigated amides (**20a–e**) (**20b**,  $K_i(hCB_2R) = 14.4$   $\mu$ M and  $IC_{50}(hBChE) = 1.2$   $\mu$ M; **Table 1**). We also introduced a “flipped” amide, where the amine moiety is directly attached to

the benzimidazole (**39**). Compound **39** is a structural isomer of **20b** and surprisingly shows a different pharmacological profile. While **20b** shows a one-digit micromolar activity at BChE and two-digit affinity at *h*CB<sub>2</sub>R (**Table 1**), **39** completely lost inhibitory activity at BChE, but the affinity toward *h*CB<sub>2</sub>R is increased compared to compound **20b** (**39**,  $K_i(hCB_2R) = 4.3$   $\mu$ M; **20b**,  $K_i(hCB_2R) = 14.4$   $\mu$ M; **Table 1**).

With another set of compounds, we investigated the influence of electron-withdrawing/donating substituents at position 5 of the benzimidazole core, which was otherwise not altered (**37** and **38**). Our assumption was based on our previous results from computational studies<sup>36</sup> that an electron-withdrawing substituent is crucial for any affinity/activity at both *h*CB<sub>2</sub>R and BChE. We could confirm this by completely losing activity at BChE and dramatically decreasing affinity at *h*CB<sub>2</sub>R when we introduced an amino moiety (**38**). Moreover, an electron-withdrawing nitro substituent (**37**) achieved a submicromolar affinity at *h*CB<sub>2</sub>R, but again it completely lost the ability to inhibit BChE (**37**,  $K_i(hCB_2R) = 961.8$  nM; **Table 1**).

For a third set, we synthesized a set of “combination” compounds using scaffolds from our lead compounds **B**, **C**, and **D** and combining them in several 2-amino benzimidazoles (**31** and **32**). With this, we obtained **32**, a combination of the *para*-phenoxy phenyl moiety from **C** and ethylene piperidinyl from **D**, and **31**, which combine the *para*-ethoxy phenyl moiety of **B** with the ethylene piperidinyl moiety of **D**. Both compounds failed to show the desired pharmacological profile though. While affinity at *h*CB<sub>2</sub>R decreased compared to the lead compounds **B–D**

Table 1. Results of the Biological Evaluation of the Inhibitory Effect of AChE/BChE and Radioligand Binding Studies at  $hCB_1R/hCB_2R$ 

No.	X	R <sup>1</sup>	R <sup>2</sup>	R <sup>3</sup>	hBChE IC <sub>50</sub> (pIC <sub>50</sub> ± SD) or % Inhibition	AChE <sup>c, d</sup> IC <sub>50</sub> (pIC <sub>50</sub> ± SD) or % Inhibition	hCB <sub>2</sub> R <sup>a</sup> K <sub>i</sub> (pIC <sub>50</sub> ± SD) or [ <sup>3</sup> H]CP55,950 displ. at 10 μM	hCB <sub>1</sub> R <sup>b</sup> K <sub>i</sub> (pIC <sub>50</sub> ± SD) or [ <sup>3</sup> H]CP55,950 displ. at 10 μM
Tacrine					9.1 nM (8.0 ± 0.0)	18.5 nM <sup>c</sup> (7.7 ± 0.0)	n.d.	n.d.
Rimonabant					n.d.	n.d.	4.0%	143.0 nM (6.8 ± 0.1) 25.0 nM <sup>49</sup>
SR-144,528					n.d.	n.d.	19.7 nM (7.7 ± 0.1) 5.6 nM <sup>50</sup>	687.0 nM (6.1 ± 0.1) 254.0 nM <sup>50</sup>
A	CH <sub>2</sub>	NEt <sub>2</sub>			2 % at 10 μM	6 % <sup>c</sup> at 100 μM	36.7 nM <sup>36</sup> (7.4 ± 0.1)	24 % <sup>36</sup>
B	NH	NEt <sub>2</sub>			3 % at 10 μM	13 % <sup>c</sup> at 10 μM	1.9 μM <sup>36</sup> (5.7 ± 0.1)	13 % <sup>36</sup>
C	NH	NEt <sub>2</sub>			0 % at 10 μM	3 % <sup>c</sup> at 10 μM	426.0 nM <sup>36</sup> (6.3 ± 0.2)	45 % <sup>36</sup>
D	CH <sub>2</sub>	NEt <sub>2</sub>			36.8 μM (4.4 ± 0.1)	12 % <sup>c</sup> at 10 μM	188.0 nM <sup>36</sup> (6.7 ± 0.1)	14 % <sup>36</sup>
20a	CH <sub>2</sub>				1.6 μM (5.8 ± 0.1)	3 % <sup>d</sup> at 25 μM 11 % <sup>c</sup> at 10 μM	763.6 nM (6.1 ± 0.1)	37 %
20b	CH <sub>2</sub>				1.2 μM (5.9 ± 0.1)	2 % <sup>d</sup> at 10 μM 5 % <sup>c</sup> at 10 μM	14.4 μM (4.8 ± 0.2)	18 %
20c	CH <sub>2</sub>				5.2 μM (5.3 ± 0.1)	9 % <sup>d</sup> at 10 μM 6 % <sup>c</sup> at 10 μM	1.9 μM (5.7 ± 0.5)	39 %
20d	CH <sub>2</sub>				5.7 μM (5.2 ± 0.1)	8 % <sup>d</sup> at 10 μM 2 % <sup>c</sup> at 10 μM	384.5 nM (6.4 ± 0.4)	17.0 μM (4.8 ± 0.2)
20e	CH <sub>2</sub>				1 % at 10 μM	5 % <sup>d</sup> at 10 μM	4.7 μM (5.3 ± 0.4)	31 %
23	CH <sub>2</sub>	NEt <sub>2</sub>			2.7 μM (5.6 ± 0.1)	20.5 μM <sup>d</sup> (4.7 ± 0.2) 60.1 μM <sup>c</sup> (4.2 ± 0.2)	4.8 μM (5.3 ± 0.2)	2 %

(**31**,  $K_i(hCB_2R) = 10.4 \mu M$ ; **32**,  $K_i(hCB_2R) = 8.9 \mu M$ ), both compounds completely lost inhibitory activity at BChE. Nevertheless, both compounds are still selective  $hCB_2R$  ligands. Compound **30**

was developed by using the 2-amino benzimidazole scaffold from lead compound **B** and changing the *para*-ethoxy phenyl to a *para*-ethoxy benzyl moiety. With the additional methylene

Table 1. continued

No.	X	R <sup>1</sup>	R <sup>2</sup>	R <sup>3</sup>	<i>h</i> BChE IC <sub>50</sub> (pIC <sub>50</sub> ± SD) or % Inhibition	AChE <sup>c, d</sup> IC <sub>50</sub> (pIC <sub>50</sub> ± SD) or % Inhibition	<i>h</i> CB <sub>2</sub> R <sup>a</sup> K <sub>i</sub> (pIC <sub>50</sub> ± SD) or [ <sup>3</sup> H]CP55,950 displ. at 10 μM	<i>h</i> CB <sub>1</sub> R <sup>b</sup> K <sub>i</sub> (pIC <sub>50</sub> ± SD) or [ <sup>3</sup> H]CP55,950 displ. at 10 μM
24	CH <sub>2</sub>	NEt <sub>2</sub>			8.2 μM (5.1 ± 0.1)	11.9 μM <sup>d</sup> (4.9 ± 0.1)  20.0 μM <sup>c</sup> (4.7 ± 0.1)	1.0 μM (5.9 ± 0.1)	4 %
30	NH	NEt <sub>2</sub>			4 % at 50 μM	7 % <sup>d</sup> at 50 μM	353.4 nM (6.4 ± 0.1)	21 %
31	NH	NEt <sub>2</sub>			53.4 μM (4.3 ± 0.1)	18 % <sup>d</sup> at 100 μM  3 % <sup>c</sup> at 10 μM	10.4 μM (4.9 ± 0.2)	17 %
32	NH	NEt <sub>2</sub>			4 % at 25 μM	3 % <sup>d</sup> at 25 μM	8.9 μM (5.1 ± 0.2)	37 %
37	CH <sub>2</sub>	NO <sub>2</sub>			12 % at 50 μM	14 % <sup>d</sup> at 50 μM	961.8 nM (6.0 ± 0.2)	41 %
38	CH <sub>2</sub>	NH <sub>2</sub>			39 % at 100 μM	15 % <sup>d</sup> at 100 μM	21.0 μM (4.7 ± 0.1)	27 %
39	CH <sub>2</sub>				25 % at 10 μM	2 % <sup>d</sup> at 10 μM	4.3 μM (5.4 ± 0.4)	36 %

<sup>a</sup>Screened on membranes of HEK cells stably expressing *h*CB<sub>2</sub>R using 10 μM of the compound; values are mean values from at least 2 independent experiments performed in triplicates. *K<sub>i</sub>* value was determined when displacement of [<sup>3</sup>H] CP 55,940 was >50%, mean values of at least 2 independent experiments performed in triplicates. <sup>b</sup>Screened on membranes of CHO cells stably expressing *h*CB<sub>1</sub>R using 10 μM of the compound; values are mean values from at least 2 independent experiments performed in triplicates. *K<sub>i</sub>* value was determined when displacement of [<sup>3</sup>H] CP 55,940 was >50%, mean values of at least 2 independent experiments. <sup>c</sup>Values are means of at least three determinations. AChE from human erythrocytes. n.d. = not determined <sup>d</sup>Values are means of at least three determinations. AChE from electric eel. Also included in this table, see references 36, 49, and 50.

group, a higher degree of freedom is achieved and the conjugated system is interrupted, which may increase basicity and thereby interaction with BChE. Compared to lead compound **B**, affinity toward *h*CB<sub>2</sub>R increased; selectivity was kept (**30**, *K<sub>i</sub>*(*h*CB<sub>2</sub>R) = 353.4 nM), but again inhibition of both ChEs was lost.

On the basis of our previous computational studies, which indicated a binding cavity in the oxyanion hole of the BChE and the *N*<sup>1</sup>-alkyl chain pointing toward it,<sup>36</sup> we changed the length of the ethylene piperidinyl moiety of our lead structure **D**. We synthesized *N*<sup>1</sup>-substituted benzimidazoles with a butylene (**23**) and a hexylene spacer (**24**) with the aim to increase lipophilicity and interactions between the side chain and the oxyanion hole of the BChE. Compared to the structurally similar lead compound **D** with an ethylene spacer, both compounds **23** and **24** show an approximately 10-fold decreased affinity toward *h*CB<sub>2</sub>R (**23**, *K<sub>i</sub>*(*h*CB<sub>2</sub>R) = 4.8 μM; **24**, *K<sub>i</sub>*(*h*CB<sub>2</sub>R) = 1.0 μM; Table 1), with an improved selectivity over *h*CB<sub>1</sub>R. Regarding BChE, both compounds indeed showed a low micromolar activity at BChE (**23**, IC<sub>50</sub>(*h*BChE) = 2.7 μM; **24**, IC<sub>50</sub>(*h*BChE) = 8.2 μM; Table 1) but lose selectivity over AChE with longer alkylene spacers

(**23**, IC<sub>50</sub>(*ee*AChE) = 20.5 μM; **24**, IC<sub>50</sub>(*ee*AChE) = 11.9 μM; Table 1). When tested at the *h*AChE, both compounds showed a similar inhibitory activity (**23**, IC<sub>50</sub>(*h*AChE) = 60.1 μM; **24**, IC<sub>50</sub>(*h*AChE) = 20.0 μM; Table 1).

Since lead compounds **A–D** were previously only tested at the *eq*BChE and *ee*AChE (Figure 1), we also investigated activity at both human enzymes, *h*BChE and *h*AChE. Surprisingly, lead compounds **A–D**, which showed a (sub)micromolar activity at *eq*BChE, completely lost significant activity at *h*BChE. In contrast, values for *h*AChE were very similar to the *ee*AChE (Figure 1 and Table 1). We recommend using the human enzyme whenever possible, which is in the literature rarely done in the development of BChE inhibitors, probably due to its high price.<sup>27b</sup> Some heterocyclic templates can show pronounced differences in inhibitory activities between species, so for each template, we recommend at least to test representative compounds at *h*BChE to check whether interspecies-dependent BChE inhibition occurs.<sup>27c</sup>

We were able to successfully develop a set of second-generation benzimidazole/2-aminobenzimidazole compounds, which nearly all show good selectivity for both *h*CB<sub>2</sub>R and *h*BChE

with affinity/activity in the micromolar to submicromolar range. Furthermore, our best compounds show a well-balanced activity profile at both targets. A balanced profile is one of the main difficulties in designing merged dual-active compounds.

For a better comparison of all compounds and investigating/describing SARs, we correlated  $pK_i$  values from  $hCB_2R$  and  $pIC_{50}$  values from  $hBChE$  in Figure 3. Interpretation is greatly

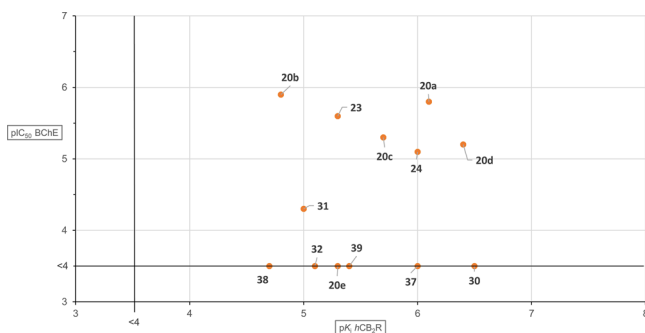


**Figure 3.** Plot of  $IC_{50}$  values for  $hBChE$  inhibition against  $pK_i$  values of  $hCB_2R$  affinity. Compounds with no significant affinity for one of the targets are placed on the black lines.

simplified by the fact that the majority of compounds still show a high selectivity over both  $hCB_1R$  and  $AChE$ .

### Computational Studies, Construction of the Active-State Model of the $hCB_2R$ , and Docking of Compounds

**20a and 20d.** Computationally driven multitarget drug discovery has emerged recently as a subfield of computational drug design, and it uses fragment-based approaches to identify multitarget hits in silico or deals with optimizing multitarget hits, e.g., by application of molecular dynamics (MD) [ref 51 and references cited herein].

Within a previous study, an active state model of the  $hCB_2R$  was constructed based on the crystal structure of the active human  $\beta_2R$  adrenergic receptor ( $h\beta_2R$ ).<sup>36</sup> Since a crystal structure of the  $hCB_1R$  in complex with the agonist AM11542 ((6aR,10aR)-3-(8-bromanyl-2-methyl-octan-2-yl)-6,6,9-trimethyl-6a,7,10,10a-tetrahydrobenzo[*c*]chromen-1-ol) was published (PDB ID: 5XRA),<sup>52</sup> a new homology model of the  $hCB_2R$  based on this crystal structure was constructed because the homology between the  $hCB_2R$  and the  $hCB_1R$  is considerably higher than between the  $hCB_2R$  and the  $h\beta_2R$ . For the alignment of the amino acid sequences between the  $hCB_1R$  and the  $hCB_2R$  (Figure 4), the most conserved amino acid of each transmembrane (TM) domain according to Ballesteros and Weinstein<sup>53</sup> (marked by an asterisk) was used as reference.

For homology modeling of the  $hCB_2R$ , the software package SYBYL 7.0 (Tripos Inc.) was used. The flavodoxin of the  $hCB_1R$  crystal was deleted. The first 18 amino acids of the N-terminus and the last 44 amino acids of the C-terminus were not included in the  $hCB_2R$  homology model because these parts are not solved in the crystal structure of the  $hCB_1R$ . All amino acids that were different between the sequence of the  $hCB_1R$  (inclusive

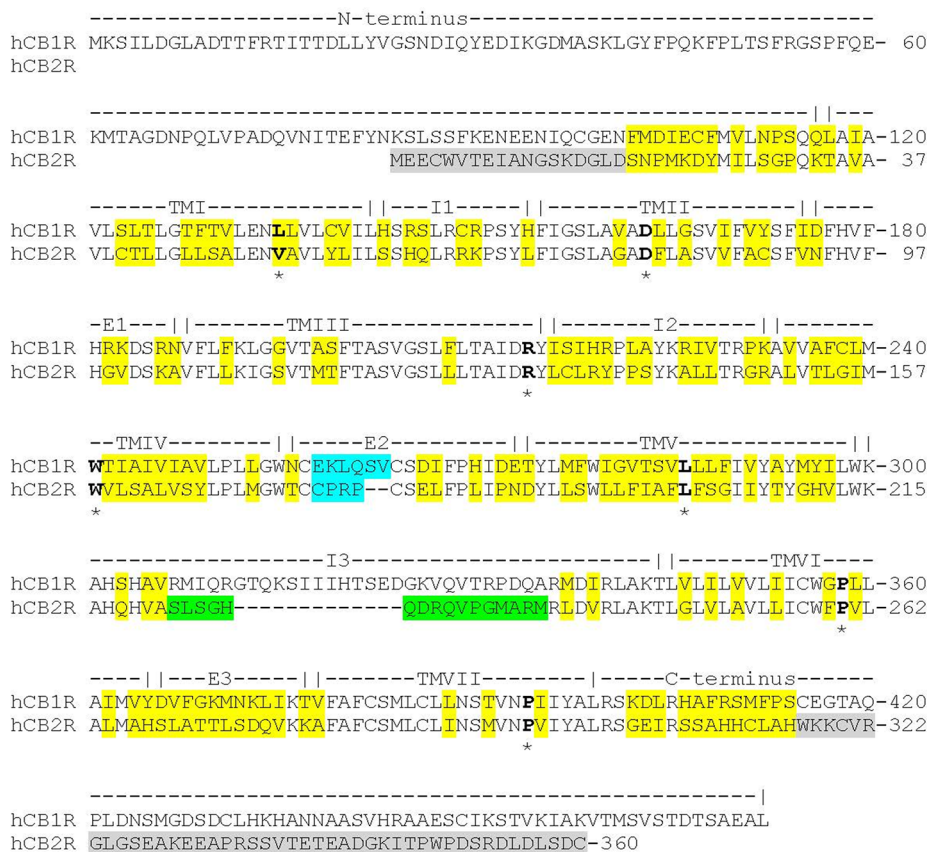


**Figure 4.** Amino acid sequence alignment of the  $hCB_1R$  (UniProtKB accession code: P21554) and the  $hCB_2R$  (UniProtKB accession code: P34972). Asterisk: highly conserved amino acids, according to the Ballesteros and Weinstein nomenclature. Yellow boxes: amino acids, different between  $hCB_1R$  and  $hCB_2R$ . Gray boxes: amino acids of the  $hCB_2R$ , not included in the homology model within the present work. Cyan boxes: part of the E2-loop, deleted in the  $hCB_1R$  template and inserted by “LoopSearch” according to the amino acid sequence of the  $hCB_2R$ . Green boxes: part of the I3-loop of the  $hCB_2R$ , inserted by “LoopSearch”.

mutations in the X-ray structure) and the *hCB<sub>2</sub>R* were mutated into the corresponding amino acid of the *hCB<sub>2</sub>R*, except these parts of the extracellular loop E2 and the intracellular loop I3, marked in Figure 4: To model the E2-loop, the amino acids Glu258 (*hCB<sub>1</sub>R*) to Val263 (*hCB<sub>2</sub>R*) were deleted and the missing amino acids of the *hCB<sub>2</sub>R* Cys175 to Pro178 were inserted, using the “LoopSearch” module of SYBYL 7.0 (Figure 4, cyan boxes). Furthermore, to model the I3-loop, the amino acids Ser222 to Met237 of the *hCB<sub>2</sub>R* were inserted, using the “LoopSearch” module of SYBYL 7.0 (Figure 4, green boxes). Compounds **20a** and **20d** were docked manually in two different poses (mode 1 and mode 2), inspired by the AM11542-*hCB<sub>1</sub>R*-crystal structure (5XRA), into the binding pocket of the *hCB<sub>2</sub>R* (Figure 5).

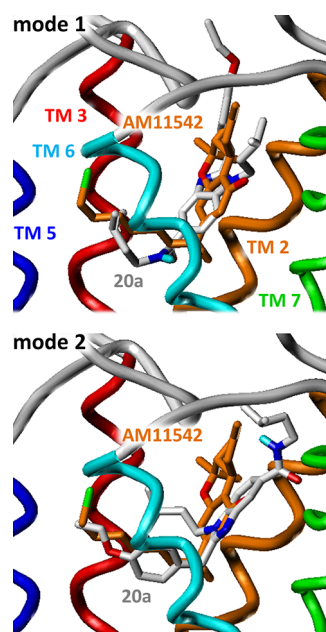


**Figure 5.** Docking poses (mode 1 and mode 2) of **20a** compared to the pose of compound AM11542 in the *hCB<sub>1</sub>R*-crystal structure (5XRA).

**Molecular Dynamics Simulations at the *hCB<sub>2</sub>R*.** The ligand–receptor complex, constructed with SYBYL 7.0, as described above was embedded in a POPC lipid bilayer. The parametrization for the ligands **20a** and **20d** was obtained from the PRODRG server (davapc1.bioch.dundee.ac.uk/prodrgr/). For the generation of the complete simulation box (6.9 nm × 6.9 nm × 9.2 nm) and subsequent molecular dynamics simulations, the software package GROMACS 4.0.2 (www.gromacs.org) was used. Intracellular and extracellular water molecules were added using the command “genbox”. To achieve electroneutrality, 5 sodium and 17 chloride ions were added using the command “genion”. After minimization of the simulation box, MD simulations (10 ns equilibration phase and 10 ns productive phase) were performed for the ligand-free *hCB<sub>2</sub>R* and the ligand–*hCB<sub>2</sub>R* complexes, as described previously.<sup>54,55</sup>

**Binding Mode of Compounds **20a** and **20d** at the *hCB<sub>2</sub>R*.** For compounds **20a** and **20d**, MD simulations for both binding modes 1 and 2 were performed. For **20a**, the short-range Coulomb and Lennard-Jones interactions amounted to ca. –19 kJ/mol and ca. –277 kJ/mol for mode 1 and ca. –44 kJ/mol and ca. –290 kJ/mol for mode 2. Similarly, for **20d**, the short-range Coulomb and Lennard-Jones interactions amounted to ca. –25 kJ/mol and ca. –246 kJ/mol for mode 1

and ca. –63 kJ/mol and ca. –260 kJ/mol for mode 2. Because mode 2 is the more stable one in both cases, subsequent data analysis was performed only on this mode. Since the orthosteric binding pocket of the *hCB<sub>2</sub>R* is mainly formed by the aromatic amino acids Phe<sup>3.36</sup>, Phe183 (E2-loop), Trp<sup>5.43</sup>, and Trp<sup>6.48</sup>, an aromatic moiety of the ligand in this region of the binding site should be preferred with respect to a more aliphatic one. Thus, for ligands containing an aromatic moiety in side chain R<sup>1</sup> and in side chain R<sup>3</sup>, e.g., **20b**, both modes should be considered.

The ligands **20a** and **20d** are stably embedded (mode 2) in the orthosteric binding pocket of the *hCB<sub>2</sub>R* (Figure 6).

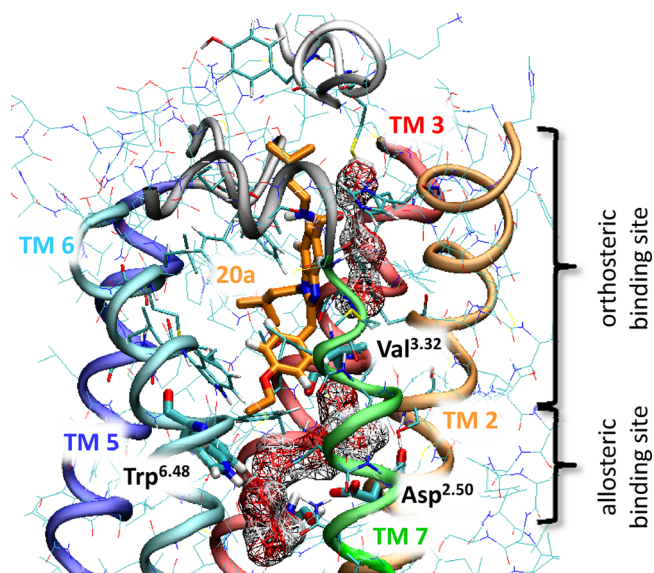


**Figure 6.** Orthosteric binding pocket of the *hCB<sub>2</sub>R* with compound **20a** as well as internal water molecules and the allosteric binding site, as obtained by MD simulations.

For compound **20a**, the benzimidazole core interacts with Phe<sup>2.57</sup>, Phe183 (E2-loop), and Phe<sup>7.35</sup> (Figure 7a). The aliphatic side chain R<sup>1</sup> is embedded in a subpocket at the extracellular domains of the *hCB<sub>2</sub>R*. The isopentyl moiety (R<sup>2</sup>) is well-embedded in a hydrophobic pocket, formed by the amino acids Ile<sup>3.29</sup>, Val<sup>3.32</sup>, Thr<sup>3.33</sup> (methyl group), Phe<sup>3.36</sup>, Phe183 (E2-loop), Ile186 (E2-loop), Leu<sup>5.40</sup>, Trp<sup>5.43</sup>, Leu<sup>5.44</sup>, Val<sup>6.51</sup>, and Met<sup>6.55</sup> (Figure 7b). The 4-ethoxybenzyl moiety (R<sup>3</sup>) is embedded in a hydrophobic pocket, mainly formed by the amino acids Phe<sup>3.36</sup>, Trp<sup>6.48</sup>, Val<sup>6.51</sup>, Met<sup>6.55</sup>, and Leu<sup>7.41</sup> (Figure 7c). During ~33% of the whole productive phase, a direct H-bond between the carbonyl oxygen of **20a** and the OH moiety of Ser<sup>7.39</sup> was observed. Alternatively, the interaction between **20a** and the *hCB<sub>2</sub>R* was stabilized by a water-mediated H-bond interaction between the CO moiety of **20a** and Ser<sup>7.39</sup> or His<sup>2.65</sup> (Figure 7d).

Furthermore, the MD simulations of the **20a**–*hCB<sub>2</sub>R* complex revealed a well-established interaction network between the highly conserved Asn<sup>7.49</sup>, Asn<sup>7.45</sup>, Trp<sup>6.48</sup>, Ser<sup>3.39</sup>, Asp<sup>2.50</sup>, and internal water molecules (Figure 8). A comparable water chain was also revealed by MD simulations for the histamine H<sub>3</sub> and H<sub>4</sub> receptor.<sup>56</sup> Thus, at the *hCB<sub>2</sub>R*, the allosteric Asp<sup>2.50</sup> binding site, which is described as the Na<sup>+</sup> binding site for several GPCRs<sup>57</sup> is well-connected with the orthosteric ligand binding site. Because the highly conserved amino acids of the allosteric binding site may be involved in receptor activation, it may be speculated that ligands (e.g., agonists), bound to the orthosteric binding site, may transfer information for activation of the receptor

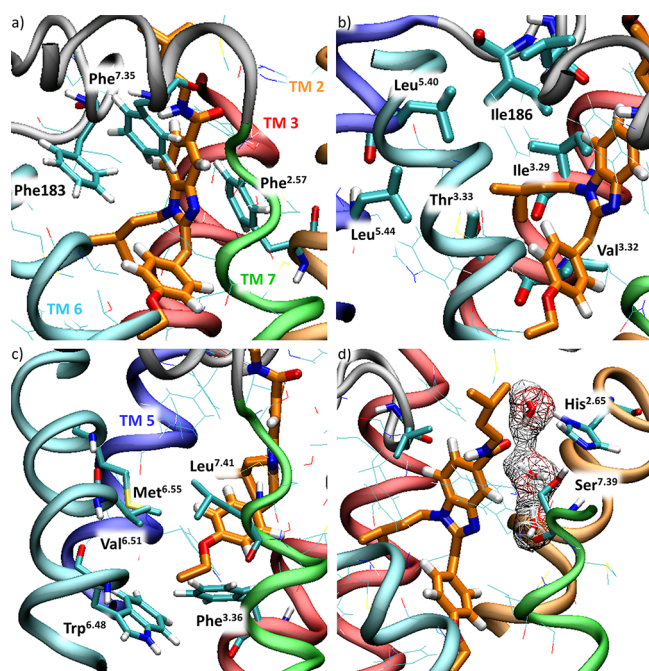


**Figure 7.** Interaction sites of the *hCB<sub>2</sub>R* with (a) the benzimidazole core, (b) the isopentyl side chain ( $R^2$ ), (c) the 4-ethoxy phenyl moiety ( $R^3$ ), and (d) the carbonyl moiety (mediated by water molecules) of compound 20a.

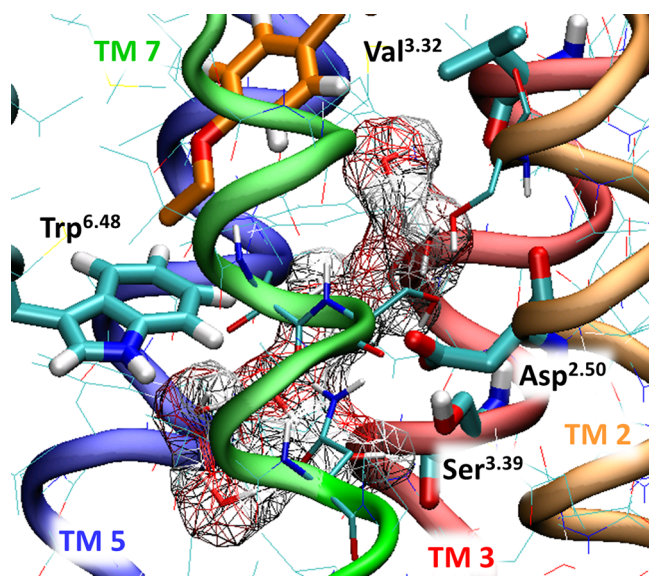


**Figure 8.** Interaction network between the *hCB<sub>2</sub>R* and internal water molecules between the orthosteric ( $\text{Val}^{3.32}$ ) and allosteric ( $\text{Asp}^{2.50}$ ) binding site, obtained by MD simulations in the presence of 20a.

downstream not only by the highly conserved amino acids but also by the internal water molecules located in this region.

Compared to 20a, the MD simulations revealed different binding modes for 20d (Figure 9): For compound 20d, the benzimidazole core interacts with  $\text{Phe}^{2.57}$ ,  $\text{Phe}^{2.61}$ ,  $\text{Phe}^{183}$  (E2-loop), and  $\text{Phe}^{7.35}$ . The piperidine moiety  $R^1$  is embedded in a subpocket at the extracellular domains of the *hCB<sub>2</sub>R*, mainly formed by the amino acids  $\text{Phe}^{2.61}$ ,  $\text{Leu}^{182}$ ,  $\text{Leu}^{6.54}$ , and  $\text{Lys}^{7.32}$  (aliphatic part). The isopentyl moiety ( $R^2$ ) is well-embedded in a hydrophobic pocket, formed by the amino acids  $\text{Val}^{2.56}$ ,  $\text{Phe}^{3.25}$ ,  $\text{Lys}^{3.28}$  (aliphatic part), and  $\text{Ile}^{3.29}$ . The 4-ethoxybenzyl moiety ( $R^3$ ) is

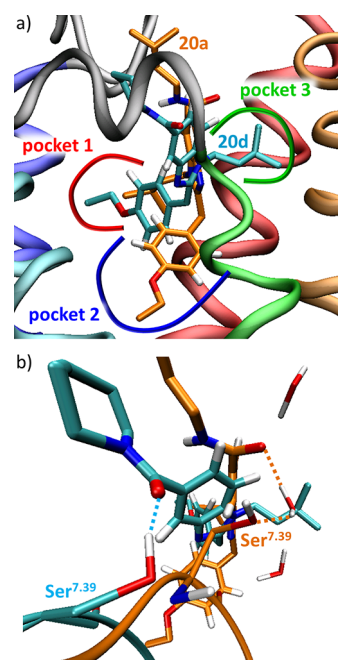


**Figure 9.** (a) Overlay of 20a and 20d in the binding pocket of the *hCB<sub>2</sub>R*, obtained by MD simulations. (b) Differences in H-bond interactions between the *hCB<sub>2</sub>R* and 20a or 20d.

embedded in a hydrophobic pocket, mainly formed by the amino acids  $\text{Ile}^{3.29}$ ,  $\text{Val}^{3.32}$ ,  $\text{Thr}^{3.33}$  (methyl group),  $\text{Phe}^{3.36}$ ,  $\text{Phe}^{183}$  (E2-loop),  $\text{Ile}^{186}$  (E2-loop),  $\text{Leu}^{5.40}$ ,  $\text{Trp}^{5.43}$ ,  $\text{Leu}^{5.44}$ ,  $\text{Val}^{6.51}$ , and  $\text{Met}^{6.55}$  (Figure 9a). During ~95% of the whole productive phase, a direct H-bond between the carbonyl oxygen and the OH moiety of  $\text{Ser}^{7.39}$  was observed. However, in contrast to 20a, the H-bond to  $\text{His}^{2.65}$  was not observed and there was no water-mediated interaction between the ligand and the receptor (Figure 9b). An overlay of 20a and 20d in the binding pocket of the *hCB<sub>2</sub>R*, obtained by MD simulations, is presented in Figure 9: The moiety  $R^1$  points for both ligands toward the extracellular region of the receptor. The isopentyl moiety ( $R^2$ ) is located in pocket 1 in the case of 20a and in pocket 3 in the case of 20d. The 4-ethoxy phenyl moiety ( $R^3$ ) is located in pocket 2 in the case of 20a and in pocket 1 in the case of 20d. Consequently, the benzimidazole core of 20d is twisted about  $45^\circ$  with respect to 20a.

Since pocket 1 ( $\text{Ile}^{3.29}$ ,  $\text{Val}^{3.32}$ ,  $\text{Thr}^{3.33}$ ,  $\text{Phe}^{3.36}$ ,  $\text{Phe}^{183}$ ,  $\text{Ile}^{186}$ ,  $\text{Leu}^{5.40}$ ,  $\text{Trp}^{5.43}$ ,  $\text{Leu}^{5.44}$ ,  $\text{Val}^{6.51}$  and  $\text{Met}^{6.55}$ ) is formed by aromatic and aliphatic side chains, ligands comprising of one or more of these moieties may be able to establish more than one binding pose. In this context two orientations of ligand 20a ( $R^2$  aliphatic) as well as 20d ( $R^3$  aromatic/aliphatic) are to be considered. Furthermore, it can be speculated that an equilibrium between different binding poses may be established depending on the chemical nature of the moieties  $R^1$ ,  $R^2$  and  $R^3$ . Since the two ligands differ in  $R^1$ , which points into the extracellular domain, this group may influence the equilibrium of different binding poses.

**Determination of Efficacy at *hCB<sub>2</sub>R*.**  $\text{CB}_2\text{Rs}$  are coupled through  $\text{G}_{i/o}$  proteins and negatively regulate adenylate cyclase, the enzyme that catalyzes the conversion of adenosine triphosphate (ATP) to cyclic adenosine monophosphate (cAMP).<sup>58</sup> One of the notable  $\text{CB}_2\text{R}$  biological responses is the regulation of intracellular cAMP levels.  $\text{CB}_2\text{R}$  agonists decrease cAMP levels and revert forskolin-stimulated cAMP production, while  $\text{CB}_2\text{R}$  antagonists/reverse agonists increase cAMP levels and enhance forskolin-stimulated cAMP production in cell lines.<sup>59</sup> So the

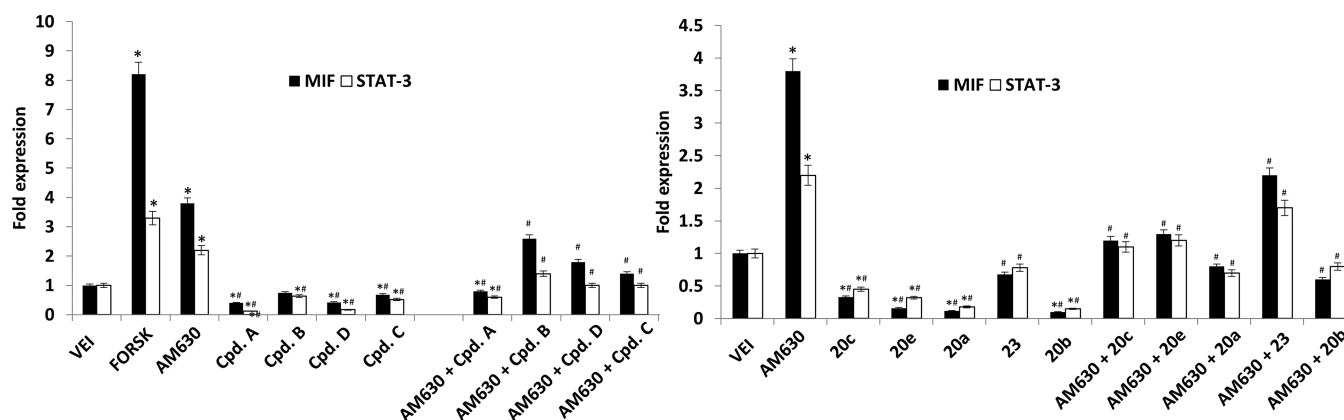


**Figure 10.** Test compounds (A–D, 20a–c, 20e, and 23) reduce MIF and STAT-3 gene expression. U266 cells were treated with test compounds (50  $\mu$ M), forskolin (10  $\mu$ M), or AM630 (25  $\mu$ M) for 2 h. In combination experiment (AM630 plus test compounds), U266 cells were preincubated with AM630 for 30 min before adding the test compounds. MIF and STAT-3 mRNA levels were determined by qRT-PCR. GAPDH was used for normalization. Data are expressed as relative fold with respect to vehicle-treated cells used as the control. Data are expressed as mean  $\pm$  SD \* $p$  < 0.01 vs untreated; # vs AM630.

detection of the cAMP concentration, for example, by ELISA, is a common method for the identification of CB<sub>2</sub>R ligand activity. In addition, receptor-mediated changes in the intracellular cAMP concentration can be detected via changes in the expression level of particular genes, which are regulated by the transcription factor cAMP response-element binding (CREB) protein binding to upstream cAMP response elements (CREs).<sup>60</sup> Between potential cAMP-target genes, macrophage migration inhibitory factor (MIF), which is highly expressed in multiple myeloma, is under cAMP-induced expression, since a functional cAMP-responsive element (CRE) in the proximal region of the MIF promoter is detected.<sup>61,62</sup> Signal transducer and activators of transcription (STAT-3) is another gene highly expressed in multiple myeloma cells, and its expression is also under CRE promoter control.<sup>63,64</sup>

Before evaluating the CB<sub>2</sub>R activity of the compounds, the nontoxic concentration of each compound was evaluated by an MTT assay, and the IC<sub>50</sub> values were determined. U266 myeloma cells were treated with different concentrations of each compound (up to 100  $\mu$ M) for 48 h, and the cell viability was calculated. As shown in Figure S1 of the Supporting Information, the compounds show different cytotoxic activity in U266 cells, with each IC<sub>50</sub> value over 40  $\mu$ M, calculated at 48 h post-treatment.

To evaluate the biological activity of the compounds (as agonist or antagonist/reverse agonist), a cAMP assay was applied. U266 cell lines were treated for 2 h with forskolin (10  $\mu$ M) as the cAMP-inducer, AM630 (25  $\mu$ M) as the CB<sub>2</sub>R antagonist/reverse agonist or with test compounds (50  $\mu$ M) alone, and in combination with AM630, respectively. In combination treatment, U266 cells were pretreated with AM630 for 30 min and then treated with the single test compounds. In the cAMP assay, we found that forskolin increased the cAMP levels (as expected) and so did AM630 (by inhibiting CB<sub>2</sub>R basal activity), compared to vehicle-treated cells (Figure S2 of the Supporting Information).

All of the test compounds decreased cAMP levels compared to vehicle, indicating that they are CB<sub>2</sub>R agonists. To further confirm this data, test compounds were incubated in competition with AM630, and the results revealed that the compounds were able to revert AM630-increased cAMP levels (Figure S2 of the Supporting Information). By summarizing these results, we confirmed that test compounds A–D act, with different potency, as CB<sub>2</sub>R agonists.

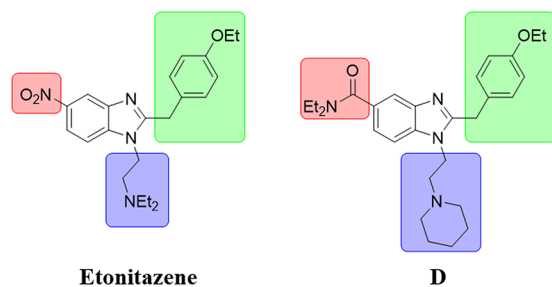
Since changes in the cAMP concentration can be detected via changes in expression level of specific genes regulated by the

CREB binding to upstream cAMP response elements (CREs), we selected two genes that are under cAMP-regulated transcription, the macrophage migration inhibitory factor (MIF) and the signal transducer and activator of transcription 3 (STAT-3). First, U266 cells were treated with forskolin to confirm that MIF and STAT-3 are under cAMP-induced transcription. As shown, both gene levels increase compared with vehicle-treated cells (Figure 10), confirming that this assay can show changes in the cAMP levels. Then, U266 cells were treated with test compounds A–D alone and in combination with AM630. The results show that AM630 increases the expression of MIF and STAT-3, confirming that AM630 increases the cAMP levels (Figure 10), as previously evidenced by cAMP ELISA, while all of our test compounds reduced MIF and STAT-3 expression levels compared with vehicle-treated cells and reduced AM630-induced MIF and STAT-3 when coincubating our test compounds and AM630 (Figure 10).

Herein, we confirmed that AM630 was able to increase cAMP production in U266 cells and that all compounds tested were able to reduce basal cAMP levels and to reverse the AM630-induced increase of cAMP concentration. An additional sensitive tool for evaluating variation in intracellular cAMP levels is the detection of CREB-induced gene expression.<sup>65,66</sup> In this context, the transcription of two genes highly expressed in U266 cells, MIF and STAT-3, were found to be under CREB regulation.<sup>62,63</sup> So, we applied a RT/PCR methodology to evaluate the MIF and STAT-3 gene expression levels in U266 cells. This experimental approach confirmed that AM630 as well as forskolin, by increasing the cAMP levels, induced MIF and STAT-3 expression, while test compounds reduced MIF and STAT-3 gene expression levels both when used alone or when combined with AM630. Since all of this data was strongly evidenced by cAMP ELISA and RT/PCR, we were able to characterize the agonist activity of test compounds and this data provides evidence that the entire set of test compounds acts as CB<sub>2</sub>R agonists, further confirming the data obtained by the cAMP ELISA assay.

**$\mu$ -Opioid Receptor Binding.** As already described above, dual-acting compounds have been developed to be applied for a variety of different targets in various diseases. One example is merged/dual-acting  $\mu$ -opioid (MOP) receptor agonists/neuronal nitric oxide synthase (nNOS) inhibitors for the treatment of pain. Such a set of compounds was designed by Renton et al. on the basis of several NOS inhibitors and etonitazene, a well-known

MOP receptor agonist developed in the 1960s.<sup>67,68</sup> During the development of our own dual-acting compounds, we came across etonitazene, which shows strong structural similarities: an electron-withdrawing substituent at position 5 of the benzimidazole core (red), a 4-ethoxybenzyl moiety at position 2 (green), and a basic amine linked with an ethylene bridge to  $N^1$  (blue), with the latter structural feature only shown by some of our compounds (Figure 11). On the basis of these observations,



$$K_i(\text{MOP}) = 0.2 \text{ nM}$$

**Figure 11.** Structural similarities between etonitazene<sup>68</sup> and (exemplary) lead compound **D**: an electron-withdrawing substituent at position 5 of the benzimidazole (red), a 4-ethoxybenzyl moiety at position 2 (green), and a basic amine linked with an ethylene bridge to  $N^1$  (blue).

we tested our lead compounds **A**, **B**, and **D** in a radioligand binding assay at the MOP receptor (HEK cells transiently transfected with the  $h\text{MOP}$  receptor) to evaluate unwanted interactions with the MOP receptor and to avoid them in further compound development (Table 2).

Radioligand binding studies confirmed our assumptions. While compound **D**, with the highest structural analogy, shows a significant, albeit moderate, three-digit nanomolar binding to the MOP receptor (**D**,  $K_i(\text{MOP}) = 556.0 \text{ nM}$ ; Table 2), lead compound **A** only shows a one-digit micromolar affinity (**A**,  $K_i(\text{MOP}) = 6.7 \text{ }\mu\text{M}$ ; Table 2). This is probably due to the lack of a basic amine. Compound **B**, which does lack not only the basic amine but also the methylene unit between the benzimidazole core and the 4-ethoxy phenyl moiety, shows the lowest affinity at the MOP receptor (**B**,  $K_i(\text{MOP}) = 53.6 \text{ }\mu\text{M}$ ; Table 2). Based on these observations for “designing out” the MOP affinity, a basic amine

attached over an alkylene linker to  $N^1$  should advantageously be avoided and the methylene unit should be substituted by a 2-amino moiety. Substitution/removal of the electron-withdrawing amide function at position 5 should be avoided to keep affinity/activity at  $h\text{CB}_2\text{R}$  and BChE as discussed above (cf. Table 1 and ref 36).

**In Vivo Studies.** Lead compounds **A** and **B** and compound **20a** were tested for their neuroprotectant and pro-cognitive effects in the in vivo mouse model of AD, in which neuroinflammation and cognitive deficits are induced by the intracerebroventricular injection of the oligomerized  $A\beta_{25-35}$  peptide into the mouse brains.<sup>28,69,70</sup>

Each compound was solubilized in DMSO/saline or DMSO/Tween-80/saline vehicle solutions (cf. Supporting Information for detailed description). Compounds were fully dissolved, and no precipitation was observed. Extended (in vitro) pharmacokinetic studies were not conducted since they are beyond the scope of this work.<sup>71</sup>

The prepared compounds were injected intraperitoneally between day 1 and 7. Animal status and weight were checked daily during the treatments. Vehicle solutions, compounds **A** and **B**, did not affect weight gains (+0.3 g/day on average). Compound **20a** decreased weight gain (+0.2 g/day at 0.3 mg/kg, +0.1 g/day at 1 mg/kg, and 0 g/day at 3 mg/kg) but did not provoke weight loss. No treatment induced behavioral alteration, prostration, signs of abdominal pain, or changes in the fur aspect, suggesting that high DMSO concentrations applied in some groups were well-tolerated. Moreover, since the injection period was limited and animals were used for behavioral observation 24 h after the last injection, vehicle-treated animals showed the performances expected for  $\text{Sc.A}\beta^-$  or  $A\beta_{25-35}$ -treated groups.<sup>69,70</sup> The amyloid peptide was injected on day 1 and the behavioral examination performed between day 8 and 10. All animals were then sacrificed on day 11 and their brains stored at  $-80 \text{ }^\circ\text{C}$  (Figure 12).

The spontaneous alternation performance, an index of spatial working memory, was tested on day 8 in the Y-maze test. Long-term memory response was measured on days 9 and 10 in a step-through passive avoidance test.

#### Repeated Treatment with Compounds **A**, **B**, and **20a**.

As described above, none of the treatments (ip for the compounds solubilized in DMSO/water or DMSO/Tween-80/water and ICV for peptides solubilized in water) affected the mouse body

**Table 2. Biological Evaluation of Radioligand Binding Studies at the  $h\text{MOP}$  Receptor**

No.	X	R <sup>1</sup>	R <sup>2</sup>	R <sup>3</sup>	$K_i(h\text{MOP})^a$ ( $\text{p}K_i \pm \text{SD}$ )
Etonitazene					0.2 nM <sup>68</sup>
<b>A</b>	CH <sub>2</sub>	CONEt <sub>2</sub>			6.7 $\mu\text{M}$ (5.2 $\pm$ 0.1)
<b>B</b>	NH	CONEt <sub>2</sub>			53.6 $\mu\text{M}$ (4.3 $\pm$ 0.0)
<b>D</b>	CH <sub>2</sub>	CONEt <sub>2</sub>			556.0 nM (6.3 $\pm$ 0.1)

<sup>a</sup>Screened on membranes of HEK cells transiently transfected with the  $h\text{MOP}$  receptor; values are mean values from at least 2 independent experiments performed in triplicates.

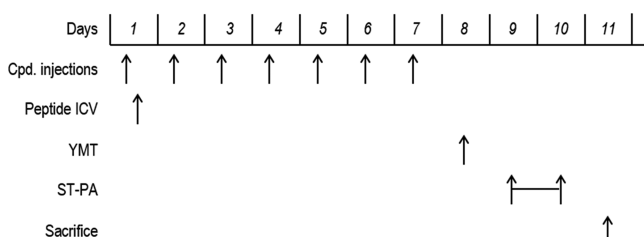


**Figure 12.** Protocol followed. Abbreviations key: Cpd, compound; ICV, intracerebroventricular injection; YMT, spontaneous alternation test in the Y-maze; ST-PA, step-through passive avoidance test.

weight, suggesting a good tolerability. Animals gained about 2.1 g during the 7 day treatment period.

**Spontaneous Alternation Performances.** CB<sub>2</sub> agonist **A** attenuated, significantly but partially, the Aβ<sub>25–35</sub>-induced alternation deficit at the highest dose tested, 3 mg/kg (Figure 13a).

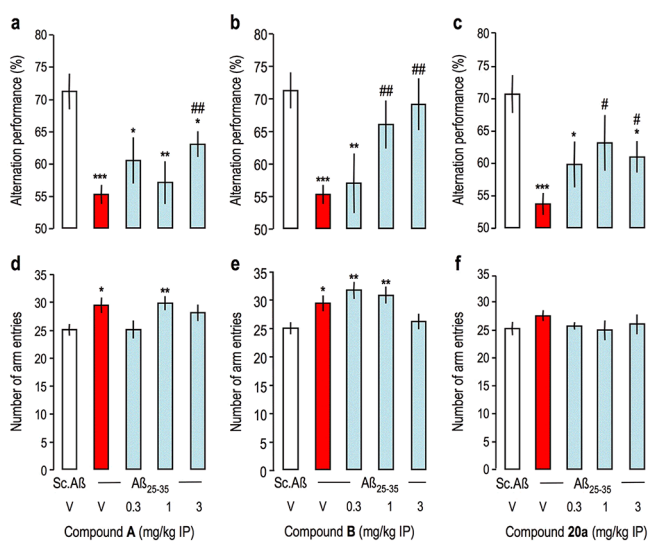


**Figure 13.** Effect of test compounds **A**, **B**, and **20a** on Aβ<sub>25–35</sub>-induced spontaneous alternation deficits in mice. Animals received Aβ<sub>25–35</sub> or Sc.Aβ peptide (9 nmol ICV) on day 1 and the test compounds (0.3 mg/kg ip) or vehicle solution (V, DMSO 20% in saline or DMSO 20%, Tween-80 2% in saline) od between days 1–7. Alternation performance was tested on day 8. Data shown mean ± SEM. ANOVA: F<sub>(4,54)</sub> = 6.55, *p* < 0.001, *n* = 9–14 per group in part a; F<sub>(4,54)</sub> = 5.43, *p* < 0.001, *n* = 8–14 per group in part b; F<sub>(4,57)</sub> = 4.05, *p* < 0.01, *n* = 9–14 per group in part c; F<sub>(4,54)</sub> = 2.72, *p* < 0.05 in part d; F<sub>(4,54)</sub> = 4.70, *p* < 0.01 in part e; F<sub>(4,57)</sub> = 0.59, *p* > 0.05 in part f. \* *p* < 0.05, \*\* *p* < 0.01, \*\*\* *p* < 0.001 vs (Sc.Aβ+V)-treated group; ## *p* < 0.01, ### *p* < 0.001 vs (Aβ<sub>25–35</sub>+V)-treated group; Dunnett's test.

Dual-acting compounds **B** and **20a** showed significant preventions at 1 and 3 mg/kg (Figure 13b,c). Note that the Aβ<sub>25–35</sub> treatment slightly, but significantly for compounds **A** and **B** (Figure 13c,d), increased locomotion, measured in terms of number of arms entered during the session, in these experiments. This is not routinely observed but remains pertinent considering the model. Slight variations with compounds **A** and **B** were noted (Figure 13c,d).

**Passive Avoidance Test.** For the long-term memory response, CB<sub>2</sub> agonist **A** failed to show any prevention of the step-through latency deficit induced by Aβ<sub>25–35</sub>, at all doses tested (Figure 14a). Dual-acting compound **B** showed significant prevention of the latency diminution at the highest dose tested,

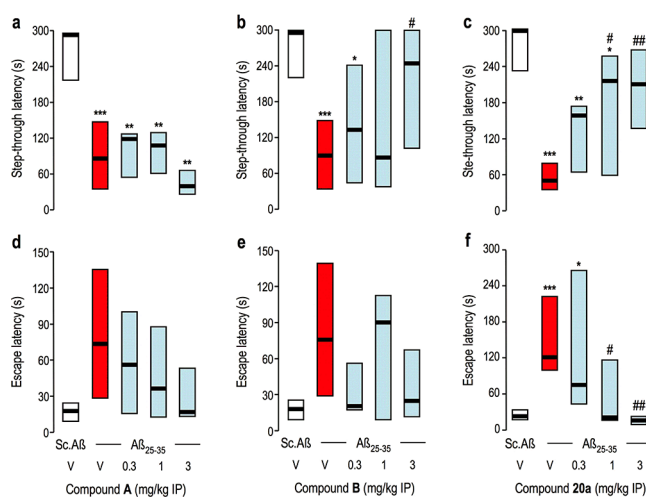


**Figure 14.** Effect of test compounds **A**, **B**, and **20a** on Aβ<sub>25–35</sub>-induced passive avoidance deficits in mice. Animals received Aβ<sub>25–35</sub> or Sc.Aβ peptide (9 nmol ICV) on day 1 and the test compounds (0.3 mg/kg ip) or vehicle solution (V, DMSO 20% in saline or DMSO 20%, Tween-80 2% in saline) od between days 1–7. Training was performed on day 9 and retention measured on day 10. Data show median and interquartile range. Kruskal–Wallis ANOVA: H = 19.0, *p* < 0.001, *n* = 9–14 per group in part a; H = 15.0, *p* < 0.01, *n* = 8–14 per group in part b; H = 21.1, *p* < 0.001, *n* = 11–14 in part c; H = 6.89, *p* > 0.05 in part d; H = 6.34, *p* > 0.05 in part e; H = 19.7, *p* < 0.001 in part f. \* *p* < 0.05, \*\* *p* < 0.01, \*\*\* *p* < 0.001 vs (Sc.Aβ+V)-treated group; # *p* < 0.05, ## *p* < 0.01 vs (Aβ<sub>25–35</sub>+V)-treated group; Dunn's test.

3 mg/kg (Figure 14b). Compound **20a** dose-dependently attenuated the step-through latency deficit induced by Aβ<sub>25–35</sub> with significant effects at 1 and 3 mg/kg (Figure 14c).

Escape latency was also measured. For compounds **A** and **B**, the Kruskal–Wallis ANOVA did not lead to significant effects (Figure 14d,e), but tendencies could be noted. The Aβ<sub>25–35</sub> treatment led to an increase in escape latency, and several groups treated with the compounds, particularly at the highest doses, showed a trend of a reduction of the latency close to the (Sc.Aβ/V) control group data (Figure 14d,e). For compound **20a**, the ANOVA was significant and the Aβ<sub>25–35</sub>-induced increase was highly significant, while the two highest doses of **20a** significantly prevented the Aβ<sub>25–35</sub>-induced increase (Figure 14f).

A protective activity for dual-acting compounds **B** and **20a** on the two behavioral responses analyzed at doses of 1–3 mg/kg was shown, and compound **20a** appeared as the most active with sustained prevention of Aβ<sub>25–35</sub>-induced learning deficits in both tests at 1 mg/kg. Since compound **A** is a potent hCB<sub>2</sub>R agonist, but weakly potent BChE inhibitor and compounds **B** and **20a** show balanced low micromolar activities at both targets, the in vivo studies prove cognition enhancement for such dual-acting compounds and, of course, also prove penetration of the blood–brain barrier. Obviously, the solubilization conditions used here remain first-attempt choices and will be improved in future studies. However, a correct bioavailability was expected for a small dual-acting compound with a much lower molecular weight compared to conventional covalently connected hybrid molecules. The compounds described herein are “true” hybrids in a way that these molecules merge the respective pharmacophores for two targets, whereas compounds termed “hybrid molecules” in the literature in the vast majority of cases covalently connect two distinct molecules that act at two different targets and therefore have a high molecular weight.<sup>34,35</sup>

## DISCUSSION AND CONCLUSION

Taken together, a compound library based on benzimidazoles and 2-aminobenzimidazoles was synthesized and SARs were investigated with respect to the  $hCB_1R$  and  $hCB_2R$  affinity and the AChE and  $hBChE$  inhibition, respectively. Generally, the compounds show excellent selectivity over both  $hCB_1R$  and AChE, and several compounds show well-balanced affinities at the two desired targets in the low micromolar range. Molecular docking and dynamics studies were performed applying for the first time a homology model of the  $hCB_2$  based on the recently published crystal structure of the  $hCB_1$  receptor bound to an agonist in the orthosteric binding site. While compound **20a** binds, as expected, to the orthosteric binding site, a stable amino acid and water interaction network was observed which extends into the allosteric binding site. Nitro-benzimidazoles can show a significant potency at the MOP receptor, and MOP affinities of dual-acting compounds could be designed out, e.g., by removing the basic nitrogen atom in the alkyl chain. Furthermore, it was proven for the first time by a cAMP assay as well as by two cAMP response elements (MIF and STAT-3) that the compounds act as agonists at the  $hCB_2R$  and might therefore exhibit antineuroinflammatory effects in vivo also. In an in vivo study with mice showing neuroinflammation and cognition deficits after  $A\beta_{25-35}$  ICV administration, the ability and superiority of a well-balanced dual-acting compound compared to a high-affinity  $hCB_2R$  agonist with moderate BChE inhibition in improving cognition at dosages from 1 to 3 mg/kg were demonstrated. This shows that it is possible to design small molecules that act specifically at two very different targets like a GPCR and an enzyme with a high selectivity and a good potency in the same concentration range to yield compounds with a pronounced in vivo activity. The development methods like compound design and application of computational methods shown in this work will hopefully provide support in related drug development efforts for dual-acting compounds.

## EXPERIMENTAL SECTION

**General Information.** All reagents were used without further purification and bought from common commercial suppliers. For anhydrous reaction conditions, THF was dried prior to use by refluxing over sodium slices for at least 2 days under an argon atmosphere. Thin-layer chromatography was performed on silica gel 60 (alumina foils with fluorescent indicator 254 nm). For detection, iodine vapor and UV light (254 and 366 nm) were used. For column chromatography, silica gel 60 (particle size 0.040–0.063 mm) was used. Nuclear magnetic resonance spectra were recorded with a Bruker AV-400 NMR instrument (Bruker, Karlsruhe, Germany) in  $CDCl_3$ , and chemical shifts are expressed in ppm relative to  $CDCl_3$  (7.26 ppm for  $^1H$  and 77.16 ppm for  $^{13}C$ ).<sup>72</sup> Purity was determined by HPLC (Shimadzu Products), containing a DGU-20A3R degassing unit, a LC20AB liquid chromatograph, and a SPD-20A UV/vis detector. UV detection was measured at 254 nm. Mass spectra were obtained by a LCMS 2020 (Shimadzu Products). As a stationary phase, a Synergi 4U fusion-RP (150 mm  $\times$  4.6 mm) column was used, and as a mobile phase, a gradient of MeOH/water with 0.1% formic acid was used. Parameters: A = water, B = MeOH,  $V(B)/(V(A) + V(B))$  = from 5% to 90% over 10 min,  $V(B)/(V(A) + V(B))$  = 90% for 5 min,  $V(B)/(V(A) + V(B))$  = from 90% to 5% over 3 min. The method was performed with a flow rate of 1.0 mL/min. Compounds were only used for biological evaluation if the purity was  $\geq 95\%$ .

**General Procedure for the Synthesis of Target Compounds 20a–e.** The respective ester compound **17** (1 equiv) was dissolved in a THF/water mixture (2:1), and LiOH (2 equiv) was added. The mixture was refluxed for 12 h. THF was evaporated, and the aqueous residue was acidified with 2 M aqueous HCl (pH = 4). The organic phase was separated with EtOAc and washed with water and brine. After the

residue was dried over  $Na_2SO_4$ , the solvent was removed in vacuo and the product was used without further purification. The respective acid (1 equiv) was dissolved in DMF, and  $NEt_3$  (1.5 equiv), HBTU (1.1 equiv), and the appropriate amine (1 equiv) were added in one portion. The mixture was stirred overnight at room temperature. Then, EtOAc and an aqueous saturated  $NaHCO_3$  solution were added. The organic layer was washed several times with water and brine and dried over anhydrous  $Na_2SO_4$ . The solvent was removed in vacuo, and the product was purified by column chromatography.

**2-(4-Ethoxybenzyl)-N,1-diisopentyl-1H-benzo[d]imidazole-5-carboxamide (20a).** **20a** was obtained as a light yellow solid (0.26 mmol, 0.11 g, 79%).  $^1H$  NMR (400 MHz,  $CDCl_3$ ):  $\delta$  = 8.08 (d,  $J$  = 1.2 Hz, 1H), 7.76 (dd,  $J$  = 8.4, 1.5 Hz, 1H), 7.23 (d,  $J$  = 8.5 Hz, 1H), 7.10 (d,  $J$  = 8.4 Hz, 2H), 6.78 (d,  $J$  = 8.5 Hz, 2H), 6.41 (s, 1H), 4.21 (s, 2H), 3.99–3.90 (m, 4H), 3.46 (dd,  $J$  = 13.8, 6.5 Hz, 2H), 1.71–1.61 (m, 1H), 1.56–1.45 (m, 3H), 1.34 (t,  $J$  = 7.0 Hz, 5H), 0.92 (d,  $J$  = 6.6 Hz, 6H), 0.86 (d,  $J$  = 6.6 Hz, 6H) ppm.  $^{13}C$  NMR (101 MHz,  $CDCl_3$ ):  $\delta$  = 167.96, 158.05, 154.83, 141.97, 137.29, 129.47, 129.05, 127.68, 122.05, 117.78, 114.86, 109.29, 63.46, 42.67, 38.56, 38.43, 38.05, 33.69, 26.11, 25.98, 22.49, 22.31, 14.75 ppm. ESI:  $m/z$  calcd for  $C_{27}H_{37}N_3O_2$   $[M + H]^+$ , 436.29; found, 436.35. HPLC purity: 98% (retention time = 11.03 min).

**2-(4-Ethoxybenzyl)-1-isopentyl-N-phenyl-1H-benzo[d]imidazole-5-carboxamide (20b).** **20b** was obtained as a light yellow solid (0.21 mmol, 92.0 mg, 64%).  $^1H$  NMR (400 MHz,  $CDCl_3$ ):  $\delta$  = 8.71–8.75 (m, 1H), 8.23 (s, 1H), 7.79–7.81 (m, 1H), 7.65–7.66 (d,  $J$  = 7.7 Hz, 2H), 7.18–7.25 (m, 3H), 6.97–7.03 (m, 3H), 6.68–6.70 (m, 2H), 4.12 (s, 2H), 3.84–3.90 (m, 4H), 1.18–1.30 (m, 6H), 0.79–0.81 (d,  $J$  = 6.6 Hz, 6H) ppm.  $^{13}C$  NMR (101 MHz,  $CDCl_3$ ):  $\delta$  = 166.40, 158.20, 155.00, 141.04, 138.74, 137.33, 129.61, 129.01, 127.31, 124.18, 122.82, 120.36, 118.06, 114.96, 109.78, 63.57, 42.93, 38.06, 33.52, 26.24, 22.40, 14.86 ppm. ESI:  $m/z$  calcd for  $C_{28}H_{31}N_3O_2$   $[M + H]^+$ , 442.24; found, 442.15. HPLC purity: 96% (retention time = 10.69 min).

**2-(4-Ethoxybenzyl)-N-hexyl-1-isopentyl-1H-benzo[d]imidazole-5-carboxamide (20c).** **20c** was obtained as a light yellow solid (0.15 mmol, 68.0 mg, 45%).  $^1H$  NMR (400 MHz,  $CDCl_3$ ):  $\delta$  = 8.03 (s, 1H), 7.80–7.82 (m, 1H), 7.30–7.33 (d,  $J$  = 8.5 Hz, 1H), 7.08–7.10 (d,  $J$  = 8.6 Hz, 2H), 6.75–6.77 (m, 2H), 6.46 (m, 1H), 4.25 (s, 2H), 4.00–4.04 (m, 2H), 3.90–3.96 (q,  $J$  = 7.0 Hz, 2H), 3.41–3.46 (m, 2H), 1.36–1.61 (m, 14H), 0.89–0.91 (m, 9H) ppm.  $^{13}C$  NMR (101 MHz,  $CDCl_3$ ):  $\delta$  = 167.91, 158.46, 154.92, 140.02, 136.83, 130.12, 129.85, 127.02, 122.99, 117.06, 115.18, 110.11, 63.72, 43.25, 40.51, 38.17, 33.40, 31.77, 29.85, 26.93, 26.39, 22.82, 22.54, 14.99, 14.26 ppm. ESI:  $m/z$  calcd for  $C_{28}H_{39}N_3O_2$   $[M + H]^+$ , 450.30; found, 450.25. HPLC purity: 99% (retention time = 11.23 min).

**2-(4-Ethoxybenzyl)-1-isopentyl-1H-benzo[d]imidazol-5-yl)-(piperidin-1-yl)methanone (20d).** **20d** was obtained as a light yellow solid (0.15 mmol, 68.0 mg, 45%).  $^1H$  NMR (400 MHz,  $CDCl_3$ ):  $\delta$  = 7.72 (s, 1H), 7.27–7.30 (m, 1H), 7.20–7.23 (d,  $J$  = 9.2 Hz, 1H), 7.07–7.10 (d,  $J$  = 8.7, 2H), 6.74–6.76 (m, 2H), 5.95 (s, 1H), 4.22 (s, 2H), 3.91–3.92 (m, 2H), 3.41–3.58 (br, 2H), 1.44–1.61 (m, 7H), 1.29–1.32 (m, 5H), 0.82–0.83 (d,  $J$  = 6.6 Hz, 6H) ppm.  $^{13}C$  NMR (101 MHz,  $CDCl_3$ ):  $\delta$  = 170.73, 158.22, 154.33, 135.65, 130.75, 129.63, 127.52, 122.29, 117.87, 115.02, 109.77, 63.58, 42.85, 38.12, 33.58, 26.21, 24.75, 22.42, 14.87 ppm. ESI:  $m/z$  calcd for  $C_{27}H_{35}N_3O_2$   $[M + H]^+$ , 434.27; found, 434.15. HPLC purity: 98% (retention time = 10.35 min).

**N-((3*s*,5*s*,7*s*)-Adamantan-1-yl)-2-(4-ethoxybenzyl)-1-isopentyl-1H-benzo[d]imidazole-5-carboxamide (20e).** **20e** was obtained as a light yellow solid (0.23 mmol, 113.0 mg, 70%).  $^1H$  NMR (400 MHz,  $CDCl_3$ ):  $\delta$  = 7.98 (s, 1H), 7.74–7.76 (d,  $J$  = 8.7 Hz, 1H), 7.30–7.33 (d,  $J$  = 8.7 Hz, 1H), 7.10–7.12 (m, 2H), 6.77–6.80 (m, 2H), 5.95 (s, 1H), 4.25 (s, 2H), 4.02–4.06 (m, 2H), 3.92–3.98 (d,  $J$  = 7.0 Hz, 2H), 2.14 (m, 9H), 1.72 (m, 6H), 1.54–1.61 (m, 1H), 1.35–1.39 (t,  $J$  = 7.0 Hz, 3H), 0.89–0.91 (d,  $J$  = 7.1 Hz, 6H) ppm.  $^{13}C$  NMR (101 MHz,  $CDCl_3$ ):  $\delta$  = 167.19, 158.34, 154.87, 140.19, 131.68, 129.76, 127.10, 122.52, 117.11, 115.10, 109.92, 63.64, 52.53, 43.13, 41.83, 38.12, 36.57, 33.37, 29.70, 26.29, 22.48, 14.93 ppm. ESI:  $m/z$  calcd for  $C_{32}H_{41}N_3O_2$   $[M + H]^+$ , 500.32; found, 500.25. HPLC purity: 99% (retention time = 11.77 min).

**General Procedure for the Synthesis of Target Compounds 23 and 24.** The respective bromine compound **21** or **22** (1 equiv) was

dissolved in DMF, and piperidine (2.5 equiv), Na<sub>2</sub>CO<sub>3</sub> (3 equiv), and a catalytic amount of NaI were added. The mixture was stirred at 70 °C for 12 h. After the reaction has finished, water was added and the organics were extracted with dichloromethane. The organic phase was washed several times with water and afterward dried over Na<sub>2</sub>SO<sub>4</sub>. The solvent was removed in vacuo, and the crude product was afterward purified by column chromatography using dichloromethane/methanol/NH<sub>3</sub>, aq 25% (15:1:0.1), as the eluent system.

**2-(4-Ethoxybenzyl)-N,N-diethyl-1-(4-(piperidin-1-yl)butyl)-1H-benzod[imidazole-5-carboxamide (23).** 23 was obtained as a light yellow oil (0.12 mmol, 58.0 mg, 46%). <sup>1</sup>H NMR (400 MHz, CDCl<sub>3</sub>): δ = 8.00 (s, 1H), 7.74 (t, J = 0.8 Hz, 1H), 7.29 (d, J = 0.8 Hz, 1H), 7.15 (m, 2H), 6.82 (m, 2H), 4.25 (s, 2H), 3.96–4.03 (m, 4H), 3.30–3.61 (m, 4H), 2.52 (s, 3H), 2.36 (t, J = 7.2 Hz, 2H), 1.67–1.73 (m, 2H), 1.48–1.54 (m, 4H), 1.37 (t, J = 7.2 Hz, 3H), 1.13–1.27 (m, 10H) ppm. <sup>13</sup>C NMR (101 MHz, CDCl<sub>3</sub>): δ = 171.90, 158.16, 154.57, 142.17, 135.89, 131.29, 129.66, 128.08, 121.50, 117.70, 115.01, 109.72, 63.62, 57.74, 54.00, 43.88, 33.87, 27.28, 24.62, 23.58, 22.93, 14.94 ppm. ESI: *m/z* calcd for C<sub>30</sub>H<sub>42</sub>N<sub>4</sub>O<sub>2</sub> [M + H]<sup>+</sup>, 491.34; found, 491.25. HPLC purity: 97% (retention time = 6.78 min).

**2-(4-Ethoxybenzyl)-N,N-diethyl-1-(6-(piperidin-1-yl)hexyl)-1H-benzod[imidazole-5-carboxamide (24).** 24 was obtained as a light yellow oil (0.26 mmol, 0.13 g, 70%). <sup>1</sup>H NMR (400 MHz, CDCl<sub>3</sub>): δ = 7.98 (s, 1H), 7.72 (m, 1H), 7.25–7.26 (m, 1H), 7.11 (m, 2H), 6.79 (m, 2H), 4.22 (s, 4H), 3.93–3.99 (m, 4H), 3.27–3.59 (m, 4H), 2.41 (s, 3H), 2.28 (t, J = 8 Hz, 2H), 1.58–1.65 (m, 4H), 1.50–1.53 (m, 2H), 1.39–1.47 (m, 3H), 1.35 (t, J = 7.2 Hz, 3H), 1.20 (m, 9H) ppm. <sup>13</sup>C NMR (101 MHz, CDCl<sub>3</sub>): δ = 171.88, 158.09, 154.55, 142.18, 135.98, 131.09, 129.52, 128.05, 121.34, 117.63, 114.91, 109.64, 63.54, 59.02, 54.44, 44.16, 33.87, 29.50, 27.25, 26.83, 26.26, 25.48, 24.15, 14.88 ppm. ESI: *m/z* calcd for C<sub>32</sub>H<sub>46</sub>N<sub>4</sub>O<sub>2</sub> [M + H]<sup>+</sup>, 519.37; found, 519.13. HPLC purity: 96% (retention time = 7.06 min).

**General Procedure for the Synthesis of Target Compounds 30–32.** The respective thiourea compound 27, 28, or 29 (1 equiv) was dissolved in anhydrous THF, and NEt<sub>3</sub> (1.5 equiv) and EDCI-HCl (2.5 equiv) were added. The mixture was refluxed for 3–5 h. Afterward, EtOAc was added, and the organic layer was washed with brine. The crude product was purified by column chromatography.

**2-((4-Ethoxybenzyl)amino)-N,N-diethyl-1-isopentyl-1H-benzod[imidazole-5-carboxamide (30).** The crude product was purified by column chromatography using petroleum ether and EtOAc (1:10) as eluent system. 30 was obtained as a light brown solid (0.71 mmol, 0.31 g, 38%). <sup>1</sup>H NMR (400 MHz, CDCl<sub>3</sub>): δ = 7.42 (d, J = 1.0 Hz, 1H), 7.33–7.28 (m, 2H), 7.04 (dd, J = 8.0, 1.5 Hz, 1H), 6.97 (d, J = 8.0 Hz, 1H), 6.87–6.82 (m, 2H), 4.61 (d, J = 5.3 Hz, 2H), 4.00 (q, J = 7.0 Hz, 2H), 3.79 (dd, J = 16.4, 9.0 Hz, 1H), 3.43 (d, J = 3.8 Hz, 4H), 1.61–1.49 (m, 3H), 1.39 (t, J = 7.0 Hz, 3H), 1.21–1.09 (m, 6H), 0.91 (d, J = 6.2 Hz, 6H) ppm. <sup>13</sup>C NMR (101 MHz, CDCl<sub>3</sub>): δ = 13.79, 15.10, 23.00, 25.79, 37.93, 42.33, 47.91, 64.02, 114.72, 115.46, 119.32, 121.03, 129.99, 133.41, 134.45, 141.67, 151.22, 155.09, 172.78 ppm. ESI: *m/z* calcd for C<sub>26</sub>H<sub>36</sub>N<sub>4</sub>O<sub>2</sub> [M + H]<sup>+</sup>, 437.28; found, 437.25. HPLC purity: 97% (retention time = 8.53 min).

**2-((4-Ethoxyphenyl)amino)-N,N-diethyl-1-(2-(piperidin-1-yl)ethyl)-1H-benzod[imidazole-5-carboxamide (31).** The crude product was purified by column chromatography using dichloromethane/methanol/NH<sub>3</sub>, aq 25% (50:1:0.1), as the eluent system. 31 was obtained as a light yellow solid (0.56 mmol, 0.26 g, 85%). <sup>1</sup>H NMR (400 MHz, CDCl<sub>3</sub>): δ = 7.52–7.43 (m, 3H), 7.05 (dt, J = 5.9, 3.0 Hz, 1H), 6.96 (d, J = 8.1 Hz, 1H), 6.88–6.81 (m, 2H), 3.97 (dt, J = 14.0, 4.9 Hz, 4H), 3.51–3.32 (m, 4H), 2.67 (dd, J = 5.4, 3.0 Hz, 2H), 2.51 (s, 4H), 1.68–1.59 (m, 4H), 1.54–1.42 (m, 2H), 1.38–1.32 (m, 3H), 1.23–1.02 (m, 6H) ppm. <sup>13</sup>C NMR (101 MHz, CDCl<sub>3</sub>): δ = 172.23, 154.35, 153.75, 142.04, 134.81, 133.71, 130.28, 120.74, 118.80, 115.22, 114.89, 106.63, 63.77, 55.27, 53.48, 43.24, 41.56, 25.84, 23.75, 14.91, 13.85 ppm. ESI: *m/z* calcd for C<sub>27</sub>H<sub>37</sub>N<sub>5</sub>O<sub>2</sub> [M + H]<sup>+</sup>, 464.29; found, 464.15. HPLC purity: 96% (retention time = 6.18 min).

**N,N-Diethyl-2-((4-phenoxyphenyl)amino)-1-(2-(piperidin-1-yl)ethyl)-1H-benzod[imidazole-5-carboxamide (32).** The crude product was purified by column chromatography using dichloromethane/methanol/NH<sub>3</sub>, aq 25% (50:1:0.1), as the eluent system. 32 was

obtained as a light brown solid (0.82 mmol, 0.42 g, 61%). <sup>1</sup>H NMR (400 MHz, CDCl<sub>3</sub>): δ = 7.59–7.51 (m, 2H), 7.43 (d, J = 1.1 Hz, 1H), 7.25–7.16 (m, 2H), 7.03 (dt, J = 8.7, 4.3 Hz, 1H), 6.99–6.86 (m, 6H), 3.98–3.90 (m, 2H), 3.46–3.22 (m, 4H), 2.67–2.61 (m, 2H), 2.49 (s, 4H), 1.65–1.55 (m, 4H), 1.50–1.41 (m, 2H), 1.14–0.98 (m, 6H) ppm. <sup>13</sup>C NMR (101 MHz, CDCl<sub>3</sub>): δ = 172.22, 158.17, 153.12, 151.41, 141.87, 136.50, 134.66, 130.44, 129.60, 122.61, 120.29, 120.24, 119.07, 118.02, 115.06, 106.84, 59.92, 55.35, 41.60, 31.62, 25.84, 23.73, 13.88 ppm. ESI: *m/z* calcd for C<sub>31</sub>H<sub>37</sub>N<sub>5</sub>O<sub>2</sub> [M + H]<sup>+</sup>, 512.29; found, 512.20. HPLC purity: 97% (retention time = 7.79 min).

**N-(2-(4-Ethoxybenzyl)-1-isopentyl-1H-benzod[imidazol-5-yl]-benzamide (39).** Benzoic acid (1 equiv) was dissolved in DMF, and NEt<sub>3</sub> (1.5 equiv), HBTU (1.1 equiv), and amine 38 (1 equiv) were added in one portion. The mixture was stirred overnight at room temperature. EtOAc and a saturated aqueous NaHCO<sub>3</sub> solution were added. The organic layer was washed several times with water and brine and dried over anhydrous Na<sub>2</sub>SO<sub>4</sub>. The solvent was removed in vacuo, and the product was purified by column chromatography using petroleum ether and EtOAc (1:2) as the eluent system. 39 was obtained as a colorless solid (0.42 mmol, 0.19 g, 64%). <sup>1</sup>H NMR (400 MHz, CDCl<sub>3</sub>): δ = 8.08–7.95 (m, 4H), 7.56–7.42 (m, 3H), 7.29 (d, J = 9.3 Hz, 1H), 7.22–7.15 (m, 2H), 6.82 (dd, J = 8.6, 4.4 Hz, 2H), 4.43 (s, 2H), 4.08–4.01 (m, 2H), 4.01–3.93 (m, 2H), 1.62–1.50 (m, 1H), 1.41–1.32 (m, 5H), 0.89 (d, J = 6.6 Hz, 6H) ppm. <sup>13</sup>C NMR (101 MHz, CDCl<sub>3</sub>): δ = 165.98, 158.21, 150.89, 134.89, 131.75, 129.82, 129.61, 128.70, 127.33, 123.31, 114.98, 110.59, 109.88, 63.51, 42.97, 37.93, 33.09, 26.15, 22.33, 14.77 ppm. ESI: *m/z* calcd for C<sub>28</sub>H<sub>31</sub>N<sub>3</sub>O<sub>2</sub> [M + H]<sup>+</sup>, 442.24; found, 442.10. HPLC purity: 99% (retention time = 9.27 min).

## ■ ASSOCIATED CONTENT

### Supporting Information

The Supporting Information is available free of charge on the ACS Publications website at DOI: 10.1021/acs.jmedchem.7b01760.

Experimental and spectral data of compounds, detailed information about the measurement of inhibition of AChE and BChE, radioligand binding studies on the hCB<sub>1</sub>R, hCB<sub>2</sub>R, and hMOP receptors, efficacy on hCB<sub>2</sub>R, information on cell culture and cell lines, statistics, animals, biochemical and histological procedures, and statistics of behavioral studies (PDF)

Molecular formula strings (CSV)

Crystal structure of the human CB1 receptor (PDB)

### Accession Codes

PDB code for the crystal structure of the human CB1 receptor in complex with agonist AM11542 is 5XRA.<sup>52</sup> This crystal structure was used for the generation of the homology model for computational studies of the human CB2 receptor in complex with compound 20a or 20d.

## ■ AUTHOR INFORMATION

### Corresponding Author

\*E-mail: michael.decker@uni-wuerzburg.de. Tel: 0049-931-31-89676.

### ORCID

Michael Decker: 0000-0002-6773-6245

### Author Contributions

The manuscript was written through contributions of all authors. All authors have given approval to the final version of the manuscript.

### Funding

M. Decker gratefully acknowledges the German Science Foundation (Deutsche Forschungsgemeinschaft) for financial support (DFG DE1546/6-3). M. Decker and T. Maurice acknowledge support from Campus France (PHC Procope), and the German

Academic Exchange Service (DAAD), the latter providing funds from the Federal Ministry of Education and Research (BMBF). The Elite Network of Bavaria (Elitenetzwerk Bayern) awarded M. Hoffmann and J. Möller PhD positions within the International Doctoral Program "Receptor Dynamics". A travel grant by the Alzheimer Forschung Initiative e.V. for D. Dolles to present this work at the ACS spring meeting in San Francisco 2017 is gratefully acknowledged.

## Notes

The authors declare no competing financial interest.

## ACKNOWLEDGMENTS

We thank O. Lockridge (University of Nebraska Medical Center) for providing human BChE. Cell lines stably expressing *hCB<sub>1</sub>R* and *hCB<sub>2</sub>R* were kindly provided by AbbVie (Chicago, IL, USA). We thank S. Kachler and Professor K.-N. Klotz (Institute of Pharmacology and Toxicology, University of Würzburg) for the technical support and workspace for radioligand binding studies.

## ABBREVIATIONS USED

A $\beta$ , amyloid  $\beta$ ; ACh, acetylcholine; AChE, acetylcholinesterase; AD, Alzheimer's disease; ANOVA, analysis of variance; APP, amyloid precursor protein; ATP, adenosine triphosphate; BChE, butyrylcholinesterase; cAMP, cyclic adenosine monophosphate; CHO, Chinese hamster ovary; CNS, central nervous system; Cpd, compound; CRE, cAMP response element; CREB, cAMP response-element binding protein; EDCI, 1-ethyl-3-(3-(dimethylamino)propyl)carbodiimide; ELISA, enzyme-linked immunosorbent assay; EtOAc, ethyl acetate; GAPDH, glyceraldehyde 3-phosphate dehydrogenase; GPCR, G-protein coupled receptor; HBTU, 2-(1*H*-benzotriazol-1-yl)-1,1,3,3-tetramethyluronium hexafluorophosphate; *hCB<sub>1/2</sub>R*, human cannabinoid receptor subtype 1/2; HEK, human embryonic kidney; *h $\beta$ <sub>2</sub>R*, human  $\beta$ <sub>2</sub>R adrenergic receptor; ICV, intracerebroventricular; ip, intraperitoneal; MD, molecular dynamics; MIF, macrophage migration inhibitory factor; MOP,  $\mu$ -opioid; MTT, 3-(4,5-dimethylthiazol-2-yl)-2,5-diphenyltetrazolium bromide; n.d., not determined; NMDA, *N*-methyl-D-aspartate receptor; nNOS, neuronal nitric oxide synthase; od, oculus dextrus; ROS, reactive oxygen species; (q)RT/PCR, (quantitative) reverse transcription polymerase chain reaction; SAR, structure-activity relationship; Sc.A $\beta$ , scrambled amyloid  $\beta$ ; STAT-3, signal transducer and activator of transcription; ST-PA, step-through passive avoidance; TM, transmembrane; V or VEL, vehicle; YMT, Y-maze test.

## REFERENCES

- (1) Prince, M.; Comas-Herrera, A.; Knapp, M.; Guerchet, M., Karagiannidou, M. *World Alzheimer Report 2016; Improving healthcare for people living with dementia; Coverage, quality and costs now and in the future*; Alzheimer's Disease International (ADI): London, 2016.
- (2) Zemek, F.; Drtinova, L.; Nepovimova, E.; Sepsova, V.; Korabecny, J.; Klimes, J.; Kuca, K. Outcomes of Alzheimer's disease therapy with acetylcholinesterase inhibitors and memantine. *Expert Opin. Drug Saf.* **2014**, *6*, 759–774.
- (3) Ballard, C.; Gauthier, S.; Corbett, A.; Brayne, C.; Aarsland, D.; Jones, E. Alzheimer's disease. *Lancet* **2011**, *377*, 1019–1031.
- (4) Duyckaerts, C.; Dickson, D. Neuropathology of Alzheimer's disease and its variants. In *Neurodegeneration: The Molecular Pathology of Dementia and Movement Disorders*; Dickson, D., Weller, R., Eds.; Wiley-Blackwell: Oxford, 2011; Vol. 2, pp 62–91.

- (5) Ferrer, I. Defining Alzheimer as a common age-related neurodegenerative process not inevitably leading to dementia. *Prog. Neurobiol.* **2012**, *97*, 38–51.

- (6) Wyss-Coray, T. Inflammation in Alzheimer disease: driving force, bystander or beneficial response? *Nat. Med.* **2006**, *12*, 1005–1015.

- (7) Perry, V. H.; Nicoll, J. A. R.; Holmes, C. Microglia in neurodegenerative disease. *Nat. Rev. Neurol.* **2010**, *6*, 193–201.

- (8) Matsuda, L. A.; Lolait, S. J.; Brownstein, M. J.; Young, A. C.; Bonner, T. I. Structure of cannabinoid receptor and functional expression of the cloned cDNA. *Nature* **1990**, *346*, 561–564.

- (9) Chiurchiù, V.; Battistini, L.; Maccarrone, M. Endocannabinoid signaling in innate and adaptive immunity. *Immunology* **2015**, *144*, 352–364.

- (10) Van Sickle, M. D.; Duncan, M.; Kingsley, P. J.; Mouihate, A.; Urbani, P.; Mackie, K.; Stella, N.; Makriyannis, A.; Piomelli, D.; Davison, J. S.; Marnett, L. J.; Di Marzo, V.; Pittmann, Q. J.; Patel, K. D.; Sharkey, K. A. Identification and functional characterization of brainstem cannabinoid CB<sub>2</sub> receptors. *Science* **2005**, *310*, 329–332.

- (11) Núñez, E.; Benito, C.; Pazos, M. R.; Barbachano, A.; Fajardo, O.; González, S.; Tolón, R. M.; Romero, J. Cannabinoid CB<sub>2</sub> receptors are expressed by perivascular microglial cells in the human brain: an immunohistochemical study. *Synapse* **2004**, *53*, 208–213.

- (12) Grünblatt, E.; Zander, N.; Bartl, J.; Jie, L.; Monoranu, C. M.; Arzberger, T.; Ravid, R.; Roggendorf, W.; Gerlach, M.; Riederer, P. Comparison analysis of gene expression patterns between sporadic Alzheimer's and Parkinson's disease. *J. Alzheimer's Dis.* **2007**, *12*, 291–311.

- (13) Solas, M.; Francis, P. T.; Franco, R.; Ramirez, M. J. CB<sub>2</sub> receptor and amyloid pathology in frontal cortex of Alzheimer's disease patients. *Neurobiol. Aging* **2013**, *34*, 805–808.

- (14) Fernández-Ruiz, J.; Romero, J.; Velasco, G.; Tolón, R. M.; Ramos, J. A.; Guzmán, M. Cannabinoid CB<sub>2</sub> receptor: a new target for controlling neural cell survival? *Trends Pharmacol. Sci.* **2007**, *28*, 39–45.

- (15) Molina-Holgado, F.; Molina-Holgado, E.; Guaza, C.; Rothwell, N. J. Role of CB<sub>1</sub> and CB<sub>2</sub> receptors in the inhibitory effects of cannabinoids on liposaccharide-induced nitric oxide release in astrocyte cultures. *J. Neurosci. Res.* **2002**, *67*, 829–836.

- (16) Sheng, W. S.; Hu, S.; Min, X.; Cabral, G. A.; Lokensgard, J. R.; Peterson, P. K. Synthetic cannabinoid WIN55,212-2 inhibits generation of inflammatory mediators by IL-1 $\beta$ -stimulated human astrocytes. *Glia* **2005**, *49*, 211–219.

- (17) Ehrhart, J.; Obregon, D.; Mori, T.; Hou, H.; Sun, N.; Bai, Y.; Klein, T.; Fernandez, F.; Tan, J.; Shytle, R. D. Stimulation of cannabinoid receptor 2 (CB<sub>2</sub>) suppresses microglial activation. *J. Neuroinflammation* **2005**, *2*, 29.

- (18) Wu, J.; Bie, B.; Yang, H.; Xu, J. J.; Brown, D. L.; Naguib, M. Activation of the CB<sub>2</sub> receptor system reverses amyloid-induced memory deficiency. *Neurobiol. Aging* **2013**, *34*, 791–804.

- (19) Martin-Moreno, A. M.; Brera, B.; Spuch, C.; Carro, E.; Garcia-Garcia, L.; Delgado, M.; Pozo, M. A.; Innamorato, N. G.; Cuadrado, A.; de Ceballos, M. L. Prolonged oral cannabinoid administration prevents neuroinflammation, lowers  $\beta$ -amyloid levels and improves cognitive performance in Tg APP 2576 mice. *J. Neuroinflammation* **2012**, *9*, 8–12.

- (20) Koppel, J.; Vingtdoux, V.; Marambaud, P.; d'Abramo, C.; Jimenez, H.; Stauber, M.; Friedman, R.; Davies, P. CB<sub>2</sub> receptor deficiency increases amyloid pathology and alters tau processing in a transgenic mouse model of Alzheimer's disease. *Mol. Med.* **2014**, *19*, 357–364.

- (21) Bisogno, T.; Oddi, S.; Piccoli, A.; Fazio, D.; Maccarrone, M. Type-2 cannabinoid receptors in neurodegeneration. *Pharmacol. Res.* **2016**, *111*, 721–730.

- (22) Davies, P.; Maloney, A. J. Selective loss of central cholinergic neurons in Alzheimer's disease. *Lancet* **1976**, *308*, 1403.

- (23) Nordberg, A.; Ballard, C.; Bullock, R.; Darreh-Shori, T.; Somogyi, M. A Review of butyrylcholinesterase as a therapeutic target in the treatment of Alzheimer's disease. *Prim. Care Companion CNS Disord.* **2013**, *15*, 2.

- (24) Darvesh, S.; Hopkins, D. A.; Geula, C. Neurobiology of butyrylcholinesterase. *Nat. Rev. Neurosci.* **2003**, *4*, 131–138.

- (25) Mesulam, M. M.; Geula, C. Butyrylcholinesterase reactivity differentiates the amyloid plaques of aging from those of dementia. *Ann. Neurol.* **1994**, *36*, 722–727.
- (26) Guillozet, A. L.; Smiley, J. F.; Mash, D. C.; Mesulam, M. M. Butyrylcholinesterase in the life cycle of amyloid plaques. *Ann. Neurol.* **1997**, *42*, 909–918.
- (27) (a) Greig, N. H.; Utsuki, T.; Ingram, D. K.; Wang, Y.; Pepeu, G.; Scali, C.; Yu, Q.-S.; Mamczarz, J.; Holloway, H. W.; Giordano, T.; Chen, D.; Furukawa, K.; Sambamurti, K.; Brossi, A.; Lahiri, D. K. Selective butyrylcholinesterase inhibition elevates brain acetylcholine, augments learning and lowers Alzheimer  $\beta$ -amyloid peptide in rodent. *Proc. Natl. Acad. Sci. U. S. A.* **2005**, *102*, 17213–17218. (b) Li, Q.; Yang, H.; Chen, Y.; Sun, H. Recent progress in the identification of selective butyrylcholinesterase inhibitors for Alzheimer's disease. *Eur. J. Med. Chem.* **2017**, *132*, 294–309. (c) Sawatzky, E.; Wehle, S.; Kling, B.; Wendrich, J.; Bringmann, G.; Sotriffer, C. A.; Heilmann, J.; Decker, M. Discovery of highly selective and nanomolar carbamate-based butyrylcholinesterase inhibitors by rational investigation into their inhibition mode. *J. Med. Chem.* **2016**, *59*, 2067–2082.
- (28) Maurice, T.; Strehaiano, M.; Siméon, N.; Bertrand, C.; Chatonnet, A. Learning performances and vulnerability to amyloid toxicity in the butyrylcholinesterase knockout mouse. *Behav. Brain Res.* **2016**, *296*, 351–360.
- (29) Kosak, U.; Brus, B.; Knez, D.; Sink, R.; Zakelj, S.; Trontelj, J.; Pisljar, A.; Slenc, J.; Gobec, M.; Zivin, M.; Tratnjek, L.; Perse, M.; Salat, K.; Podkova, A.; Filippek, B.; Nachon, F.; Brazzolotto, X.; Wieckowska, A.; Malawska, B.; Stojan, J.; Mlinaric Rascan, I.; Kos, J.; Coquelle, N.; Colletier, J.-P.; Gobec, S. Development of an *in-vivo* active reversible butyrylcholinesterase inhibitor. *Sci. Rep.* **2016**, *6*, 39495–39510.
- (30) Darvesh, S.; Hopkins, D. A.; Geula, C. Neurobiology of butyrylcholinesterase. *Nat. Rev. Neurosci.* **2003**, *4*, 131–138.
- (31) Wright, C. I.; Geula, C.; Mesulam, M.-M. Neurological cholinesterases in the normal brain and in Alzheimer's disease: relationship to plaques, tangles, and patterns of selective vulnerability. *Ann. Neurol.* **1993**, *34*, 373–384.
- (32) Morphy, R.; Rankovic, Z. Designed multiple ligands. An emerging drug discovery paradigm. *J. Med. Chem.* **2005**, *48*, 6523–6543.
- (33) (a) Nepovimova, E.; Uliassi, E.; Korabecny, J.; Pena-Altamira, L. E.; Samez, S.; Pesaresi, A.; Garcia, G. E.; Bartolini, M.; Andrisano, V.; Bergamini, C.; Fato, R.; Lamba, D.; Roberti, M.; Kuca, K.; Monti, B.; Bolognesi, M. L. Multitarget drug design strategy: quinone–tacrine hybrids designed To block amyloid- $\beta$  aggregation and to exert anticholinesterase and antioxidant effects. *J. Med. Chem.* **2014**, *57*, 8576–8589. (b) Nepovimova, E.; Korabecny, J.; Dolezal, R.; Babkova, K.; Ondrejicek, A.; Jun, D.; Sepsova, V.; Horova, A.; Hrabanova, M.; Soukup, O.; Bukum, N.; Jost, P.; Muckova, L.; Kassa, J.; Malinak, D.; Andrs, M.; Kuca, K. Tacrine–Trolox Hybrids: A novel class of centrally active, nonhepatotoxic multi-target-directed ligands exerting anticholinesterase and antioxidant activities with low *in vivo* toxicity. *J. Med. Chem.* **2015**, *58*, 8985–9003. (c) Spilovska, K.; Korabecny, J.; Nepovimova, E.; Dolezal, R.; Mezeiova, E.; Soukup, O.; Kuca, K. Multitarget tacrine hybrids with neuroprotective properties to confront Alzheimer's disease. *Curr. Top. Med. Chem.* **2017**, *17*, 1006–1026.
- (34) Nimczick, M.; Decker, M. New approaches in the design and development of cannabinoid receptor ligands: multifunctional and bivalent compounds. *ChemMedChem* **2015**, *10*, 773–786.
- (35) Dolles, D.; Decker, M. Dual-acting compounds acting as receptor ligands and enzyme inhibitors. In *Design of Hybrid Molecules for Drug Development*; Decker, M., Ed.; Elsevier: Oxford, 2017; pp 137–165.
- (36) Dolles, D.; Nimczick, M.; Scheiner, M.; Ramler, J.; Stadtmüller, P.; Sawatzky, E.; Drakopoulos, A.; Sotriffer, C.; Wittmann, H.-J.; Strasser, A.; Decker, M. Aminobenzimidazoles and structural isomers as templates for dual-acting butyrylcholinesterase inhibitors and hCB<sub>2</sub>R ligands to combat neurodegenerative disorders. *ChemMedChem* **2016**, *11*, 1270–1283.
- (37) Le Naour, M.; Akgün, E.; Yekkirala, A.; Lunzer, M. M.; Powers, M. D.; Kalyuzhny, A. E.; Portoghese, P. S. Bivalent ligands that target  $\mu$  opioid (MOP) and cannabinoid 1 (CB<sub>1</sub>) receptors are potent analgesics devoid of tolerance. *J. Med. Chem.* **2013**, *56*, 5505–5513.
- (38) Perrey, D. A.; Gilmour, B. P.; Thomas, B. F.; Zhang, Y. Toward the development of bivalent ligand probes of cannabinoid CB<sub>1</sub> and orexin OX<sub>1</sub> receptor heterodimers. *ACS Med. Chem. Lett.* **2014**, *5*, 634–638.
- (39) Lange, J. H. M.; Coolen, H. K. A.; Van der Neut, M. A. W.; Borst, A. J. M.; Stork, B.; Verveer, P. C.; Kruse, C. G. Design, synthesis, biological properties, and molecular modeling investigations of novel tacrine derivatives with a combination of acetylcholinesterase inhibition and cannabinoid CB<sub>1</sub> receptor antagonism. *J. Med. Chem.* **2010**, *53*, 1338–1346.
- (40) Montanari, S.; Scalvini, L.; Bartolini, M.; Belluti, F.; Gobbi, S.; Andrisano, V.; Ligresti, A.; Di Marzo, V.; Rivara, S.; Mor, M.; Bisi, A.; Rampa, A. Fatty acid amide hydrolase (FAAH), acetylcholinesterase (AChE), and butyrylcholinesterase (BuChE): networked targets for the development of carbamates as potential anti-Alzheimer's disease agents. *J. Med. Chem.* **2016**, *59*, 6387–6406.
- (41) Lipinski, C. A.; Lombardo, F.; Dominy, B. W.; Feeney, P. J. Experimental and computational approaches to estimate solubility and permeability in drug discovery and development settings. *Adv. Drug Delivery Rev.* **1997**, *23*, 3–25.
- (42) Stöbel, A.; Schlenk, M.; Hinz, S.; Küppers, P.; Heer, J.; Gütschow, M.; Müller, C. E. Dual Targeting of adenosine A<sub>2A</sub> receptors and monoamine oxidase B by 4H-3,1-benzothiazin-4-ones. *J. Med. Chem.* **2013**, *56*, 4580–4596.
- (43) (a) Darras, F. H.; Pockes, S.; Huang, G.; Wehle, S.; Strasser, A.; Wittmann, H.-J.; Nimczick, M.; Sotriffer, C. A.; Decker, M. Synthesis, biological evaluation, and computational studies of tri- and tetracyclic nitrogen-bridgehead compounds as potent dual-acting AChE inhibitors and hH<sub>3</sub> receptor antagonists. *ACS Chem. Neurosci.* **2014**, *5*, 225–242. (b) Khan, N.; Saad, A.; Nurulain, S. M.; Darras, F. H.; Decker, M.; Sadek, B. The dual-acting H<sub>3</sub> receptor antagonist and AChE inhibitor UW-MD-71 dose-dependently enhances memory retrieval and reverses dizocilpine-induced memory impairments in Rats. *Behav. Brain Res.* **2016**, *297*, 155–164. (c) Sadek, B.; Khan, N.; Darras, F. H.; Pockes, S.; Decker, M. The dual-acting AChE inhibitor and H<sub>3</sub> receptor antagonist UW-MD-72 reverses amnesia induced by scopolamine or dizocilpine in passive avoidance paradigm in rats. *Physiol. Behav.* **2016**, *165*, 383–391.
- (44) (a) Pagé, D.; Balau, E.; Boisvert, L.; Liu, Z.; Milburn, C.; Tremblay, M.; Wei, Z.; Woo, S.; Luo, X.; Cheng, Y.-X.; Yang, H.; Srivastava, S.; Zhou, F.; Brown, W.; Tomaszewski, M.; Walpole, C.; Hodzic, L.; St-Onge, S.; Godbout, C.; Salois, D.; Payza, K. Novel benzimidazole derivatives as selective CB<sub>2</sub> agonists. *Bioorg. Med. Chem. Lett.* **2008**, *18*, 3695–3700. (b) Cheng, Y.-X.; Tomaszewski, M.; Walpole, C.; Yang, H. Novel Compounds. WO 02/085866 A1, October 31, 2002.
- (45) González-Naranjo, P.; Pérez-Macias, N.; Campillo, N. E.; Pérez, C.; Arán, V. J.; Girón, R.; Sánchez-Robles, E.; Martín, M. I.; Gómez-Canas, M.; García-Arencibia, M.; Fernández-Ruiz, J.; Páez, J. A. Cannabinoid agonists showing BuChE inhibition as potential therapeutic agents for Alzheimer's disease. *Eur. J. Med. Chem.* **2014**, *73*, 56–72.
- (46) Munch, H.; Hansen, J. S.; Pittelkow, M.; Christensen, J. B.; Boas, U. A new efficient synthesis of isothiocyanates from amines using di-*tert*-butyl dicarbonate. *Tetrahedron Lett.* **2008**, *49*, 3117–3119.
- (47) Freitag, M.; Schemies, J.; Larsen, T.; El Gaghlab, K.; Schulz, F.; Rumpf, T.; Jung, M.; Link, A. Synthesis and biological activity of splitomicin analogs targeted at human NAD<sup>+</sup>-dependent histone deacetylases (sirtuins). *Bioorg. Med. Chem.* **2011**, *19*, 3669–3677.
- (48) Darras, F. H.; Wehle, S.; Huang, G.; Sotriffer, C. A.; Decker, M. Amine substitution of quinazolinones leads to selective nanomolar AChE inhibitors with 'inverted' binding mode. *Bioorg. Med. Chem.* **2014**, *22*, 4867–4881.
- (49) Lange, J. H. M.; van Stuijvenberg, H. H.; Coolen, H. K. A. C.; Adolfs, T. J. P.; McCreary, A. C.; Keizer, H. G.; Wals, H. C.; Veerman, W.; Borst, A. J. M.; de Looft, W.; Verveer, C.; Kruse, C. G. Bioisosteric replacements of the pyrazole moiety of rimonabant: synthesis, biological properties, and molecular modeling investigations of thiazoles, triazoles, and imidazoles as potent and selective CB<sub>1</sub> cannabinoid receptor antagonists. *J. Med. Chem.* **2005**, *48*, 1823–1838.

- (50) Yao, B. B.; Hsieh, G. C.; Frost, J. M.; Fan, Y.; Garrison, T. R.; Daza, A. V.; Grayson, G. K.; Zhu, C. Z.; Pai, M.; Chandran, P.; Salyers, A. K.; Wensink, E. J.; Honore, P.; Sullivan, J. P.; Dart, M. J.; Meyer, M. D. *In vitro* and *in vivo* characterization of A-796260: a selective cannabinoid CB<sub>2</sub> receptor agonist exhibiting analgesic activity in rodent pain models. *Br. J. Pharmacol.* **2008**, *153*, 390–401.
- (51) Bottegoni, G.; Cavalli, A. Computational Methods in Multitarget Drug Discovery. In *Design of Hybrid Molecules for Drug Development*; Decker, M., Ed.; Elsevier: Oxford, 2017; pp 239–258.
- (52) Hua, T.; Vemuri, K.; Nikas, S. P.; Laprairie, R. B.; Wu, Y.; Qu, L.; Pu, M.; Korde, A.; Jiang, S.; Ho, J. H.; Han, G. W.; Ding, K.; Li, X.; Liu, H.; Hanson, M. A.; Zhao, S.; Bohn, L. M.; Makriyannis, A.; Stevens, R. C.; Liu, Z. J. Crystal structures of agonist-bound human cannabinoid receptor CB1. *Nature* **2017**, *547*, 468–471.
- (53) Ballesteros, J. A.; Weinstein, H. Integrated methods for the construction of three-dimensional models and computational probing of structure-function relations in G protein-coupled receptors. *Methods Neurosci.* **1995**, *25*, 366–428.
- (54) Igel, P.; Geyer, R.; Strasser, A.; Dove, S.; Seifert, R.; Buschauer, A. Synthesis and structure-activity relationships of cyanoguanidine-type and structurally related histamine H<sub>4</sub> receptor agonists. *J. Med. Chem.* **2009**, *52*, 6297–6313.
- (55) Strasser, A.; Striegl, B.; Wittmann, H.-J.; Seifert, R. Pharmacological profile of histaprodifens at four recombinant H<sub>1</sub>-receptor species isoforms. *J. Pharmacol. Exp. Ther.* **2007**, *324*, 60–71.
- (56) Wittmann, H.-J.; Seifert, R.; Strasser, A. Sodium binding to hH<sub>3R</sub> and hH<sub>4R</sub> - a molecular modeling study. *J. Mol. Model.* **2014**, *20*, 2394–2404.
- (57) Strasser, A.; Wittmann, H.-J.; Schneider, E. H.; Seifert, R. Modulation of GPCRs by monovalent cations and anions. *Naunyn-Schmiedeberg's Arch. Pharmacol.* **2015**, *388*, 363–380.
- (58) Howlett, A. C.; Barth, F.; Bonner, T. I.; Cabral, G.; Casellas, P.; Devane, W. A.; Felder, C. C.; Herkenham, M.; Mackie, K.; Martin, B. R.; Mechoulam, R.; Pertwee, R. G. International Union of Pharmacology. XXVII. Classification of cannabinoid receptors. *Pharmacol. Rev.* **2002**, *54*, 161–202.
- (59) Ross, R. A.; Brockie, H. C.; Stevenson, L. A.; Murphy, V. L.; Templeton, F.; Makriyannis, A.; Pertwee, R. G. Agonist-inverse agonist characterization at CB<sub>1</sub> and CB<sub>2</sub> cannabinoid receptors of L759633, L759656 and AM630. *Br. J. Pharmacol.* **1999**, *126*, 665–672.
- (60) Williams, C. cAMP detection methods in HTS: selecting the best from the rest. *Nat. Rev. Drug Discovery* **2004**, *3*, 125–135.
- (61) Zheng, Y.; Wang, Q.; Li, T.; Qian, J.; Lu, Y.; Li, Y.; Bi, E.; Reu, F.; Qin, Y.; Drazba, J.; Hsi, E.; Yang, J.; Cai, Z.; Yi, Q. Role of myeloma-derived MIF in myeloma cell adhesion to bone marrow and chemotherapy response. *J. Natl. Cancer Inst.* **2016**, *108* (11), djw131.
- (62) Waeber, G.; Thompson, N.; Chautard, T.; Steinmann, M.; Nicod, P.; Pralong, F. P.; Calandra, T.; Gaillard, R. C. Transcriptional activation of the macrophage migration-inhibitory factor gene by the corticotropin-releasing factor is mediated by the cyclic adenosine 3',5'-monophosphate responsive element-binding protein CREB in pituitary cells. *Mol. Endocrinol.* **1998**, *12*, 698–705.
- (63) Alas, S.; Bonavida, B. Inhibition of constitutive STAT3 activity sensitizes resistant non-Hodgkin's lymphoma and multiple myeloma to chemotherapeutic drug-mediated apoptosis. *Clin. Cancer Res.* **2003**, *9*, 316–326.
- (64) Kato, K.; Nomoto, M.; Izumi, H.; Ise, T.; Nakano, S.; Niho, Y.; Kohno, K. Structure and functional analysis of the human STAT3 gene promoter: alteration of chromatin structure as a possible mechanism for the upregulation in cisplatin-resistant cells. *Biochim. Biophys. Acta, Gene Struct. Expression* **2000**, *1493*, 91–100.
- (65) Hill, S. J.; Baker, J. G.; Rees, S. Reporter-gene systems for the study of G-protein-coupled receptors. *Curr. Opin. Pharmacol.* **2001**, *1*, 526–532.
- (66) Wood, K. V. Marker proteins for gene expression. *Curr. Opin. Biotechnol.* **1995**, *6*, 50–58.
- (67) Renton, P.; Green, B.; Maddaford, S.; Rakhit, S.; Andrews, J. S. NOPiats: Novel dual action neuronal nitric oxide synthase inhibitors with  $\mu$ -opioid agonist activity. *ACS Med. Chem. Lett.* **2012**, *3*, 227–231.
- (68) Hunger, A.; Kebrle, J.; Rossi, A.; Hoffmann, K. Benzimidazol-Derivate und verwandte Heterocyclus III. Synthese von 1-Aminoalkyl-2-benzyl-nitro-benzimidazolen. *Helv. Chim. Acta* **1960**, *43*, 1032–1046.
- (69) Maurice, T.; Lockhart, B. P.; Privat, A. Amnesia induced in mice by centrally administered  $\beta$ -amyloid peptides involves cholinergic dysfunction. *Brain Res.* **1996**, *706*, 181–193.
- (70) Lahmy, V.; Meunier, J.; Malmström, S.; Naert, G.; Givalois, L.; Kim, S. H.; Villard, V.; Vamvakides, A.; Maurice, T. Blockade of Tau hyperphosphorylation and A $\beta$ 1–42 generation by the aminotetrahydrofuran derivative ANAVEX2–73, a mixed muscarinic and  $\sigma$ 1 receptor agonist, in a nontransgenic mouse model of Alzheimer's disease. *Neuropsychopharmacology* **2013**, *38*, 1706–1723.
- (71) Huang, G.; Drakopoulos, A.; Saedtler, M.; Zou, H.; Meinel, L.; Heilmann, J.; Decker, M. Cytotoxic properties of the alkaloid rutaecarpine and its oligocyclic derivatives and chemical modifications to enhance water-solubility. *Bioorg. Med. Chem. Lett.* **2017**, *27*, 4937–4941.
- (72) Gottlieb, H. E.; Kotlyar, V.; Nudelman, A. NMR chemical shifts of common laboratory solvents as trace impurities. *J. Org. Chem.* **1997**, *62*, 7512–7515.